つくば宇宙フォーラム
2016年4月20日

重力波イベント GW150914 におけるブラックホールの初期質量と合体条件

筑波大学　計算科学研究センター

梅村　雅之

超巨大ブラックホールの謎
巨大ブラックホールー銀河バルジの比例関係（マゴリアン関係）

$$M_{\mathrm{BH}} / M_{\mathrm{bulge}} \approx 0.001$$

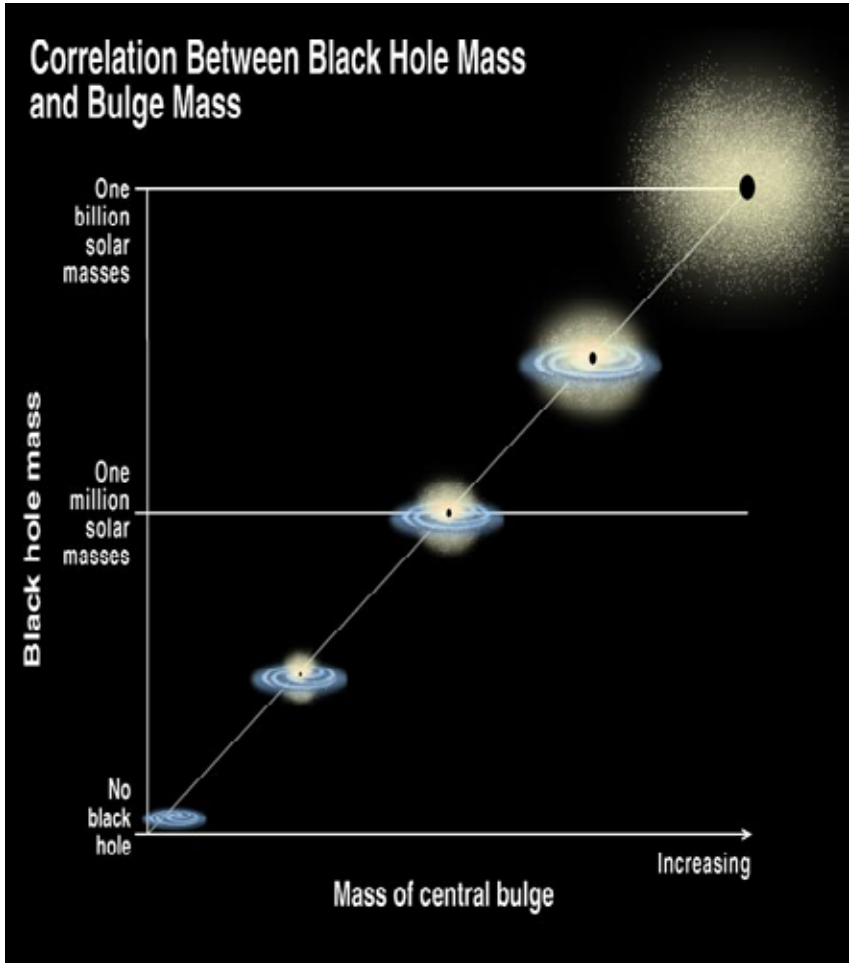

Marconi & Hunt 2003, ApJ, 589, 21

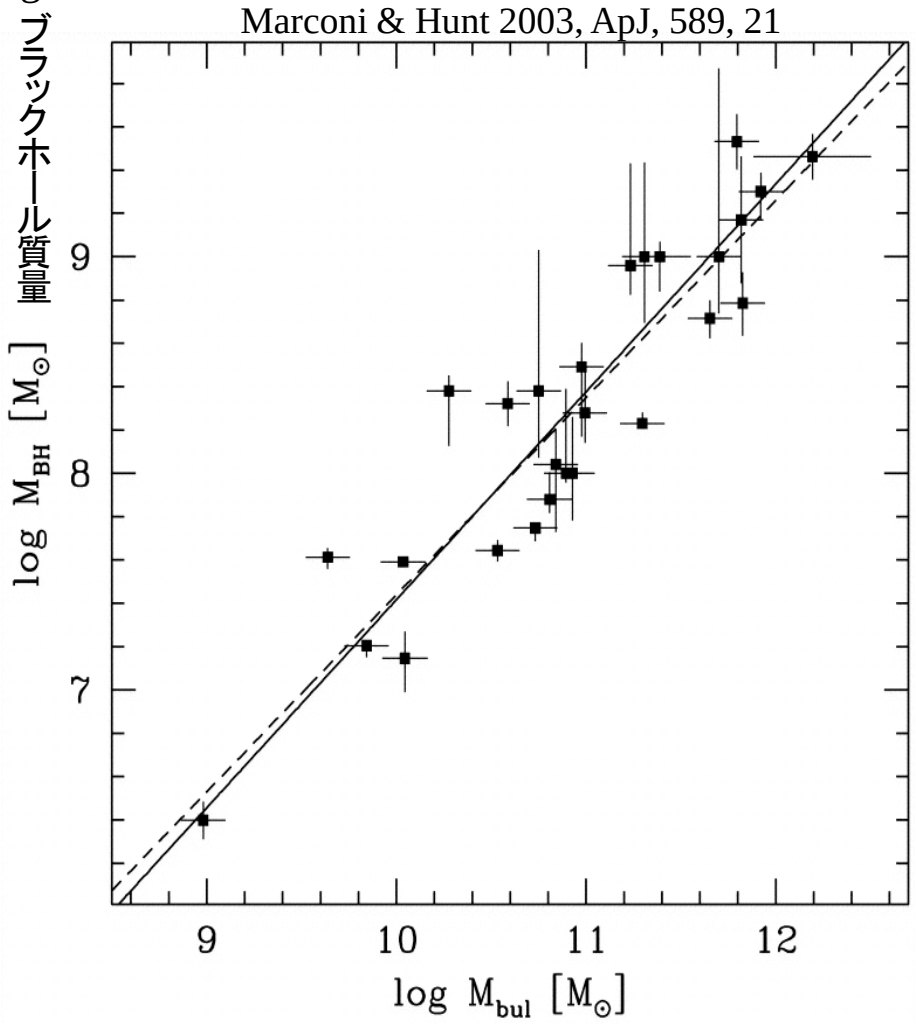

Kormendy & Richstone 1995; Magorrian et al. 1998;
Merritt & Ferrarese 2001; Marconi & Hunt 2003

Classical bulges vs Pseudo bulges

Kormendy & Ho 2013, ARA&A, 51, 511

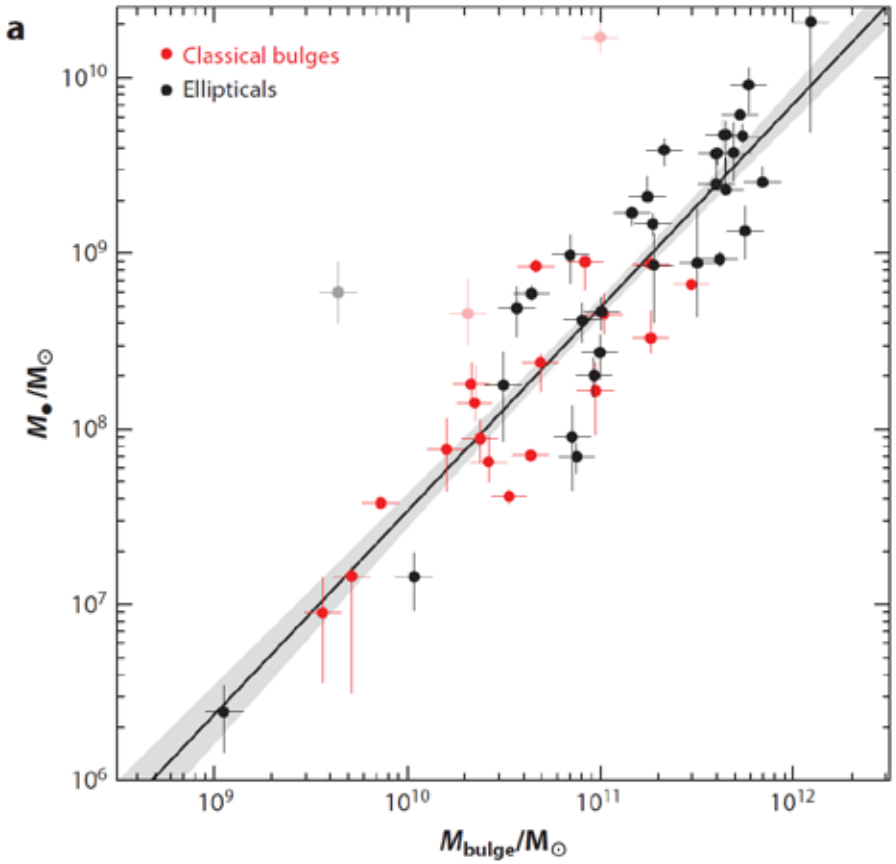

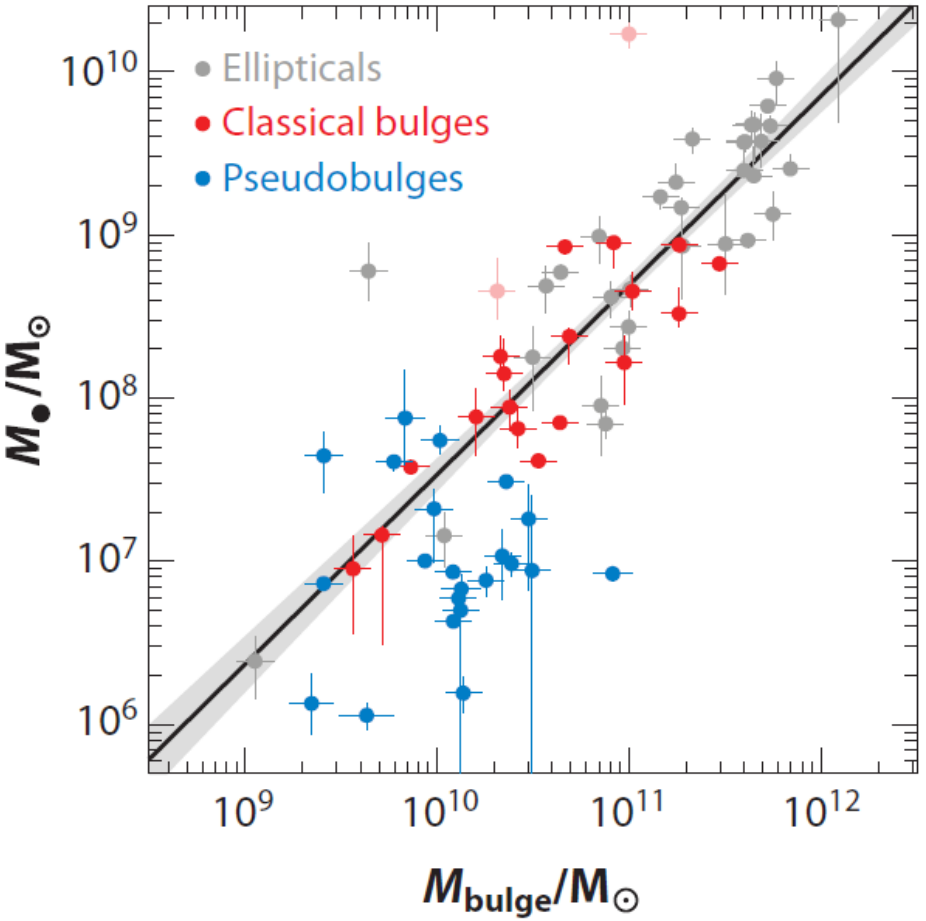

超巨大ブラックホール起源：7つの疑問

Q1：初代ブラックホールは星質量（数～10M$_\odot$）だったのか大質量（数万～数10万M$_\odot$）だったのか

Q2：Building block はどこにあるのか（宇宙論的SMBH形成）

Q3：SMBHは質量降着で成長したのか合体で成長したのか

Q4：SMBHはなぜ銀河バルジ質量の1000分の1になっているのか

Q5：SMBHは銀河中心にしかできないのか

Q6：SMBHの"ダウンサイジング"は何を意味しているのか

Q7：矮小楕円銀河にはなぜSMBHはないのか

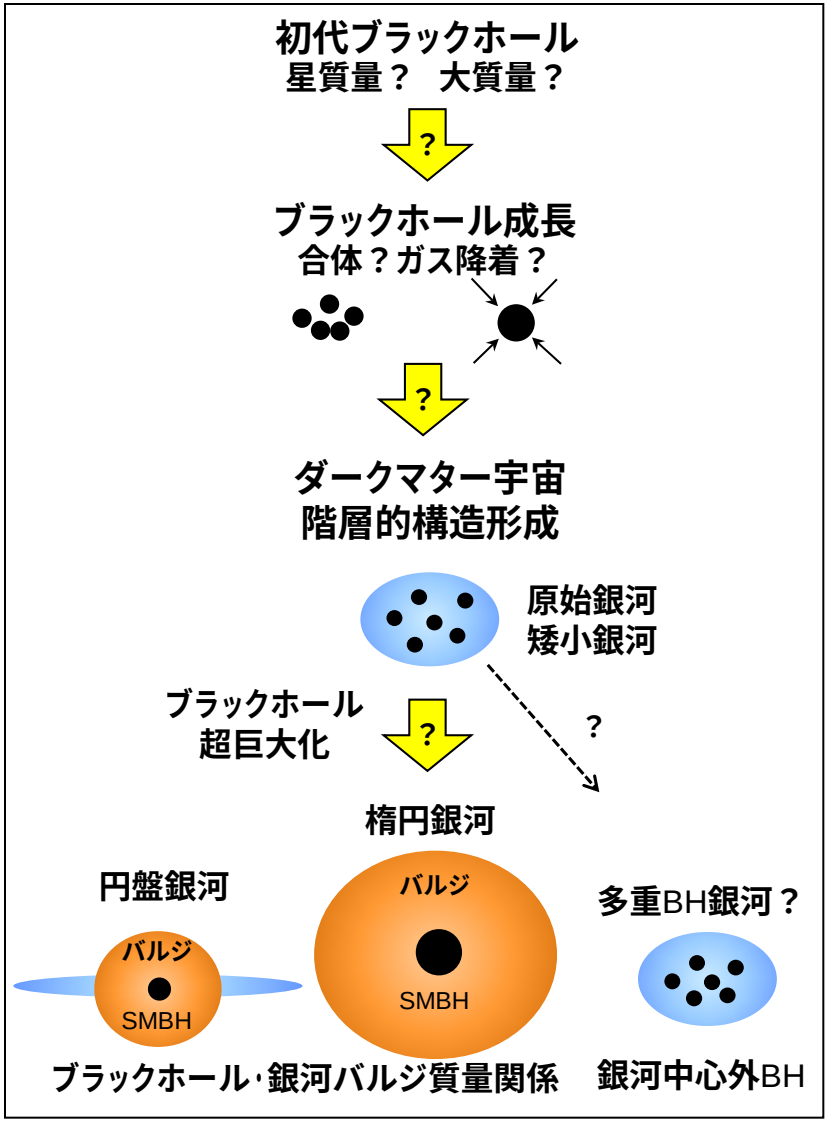

Cosmological version of Rees Diagram (1984)

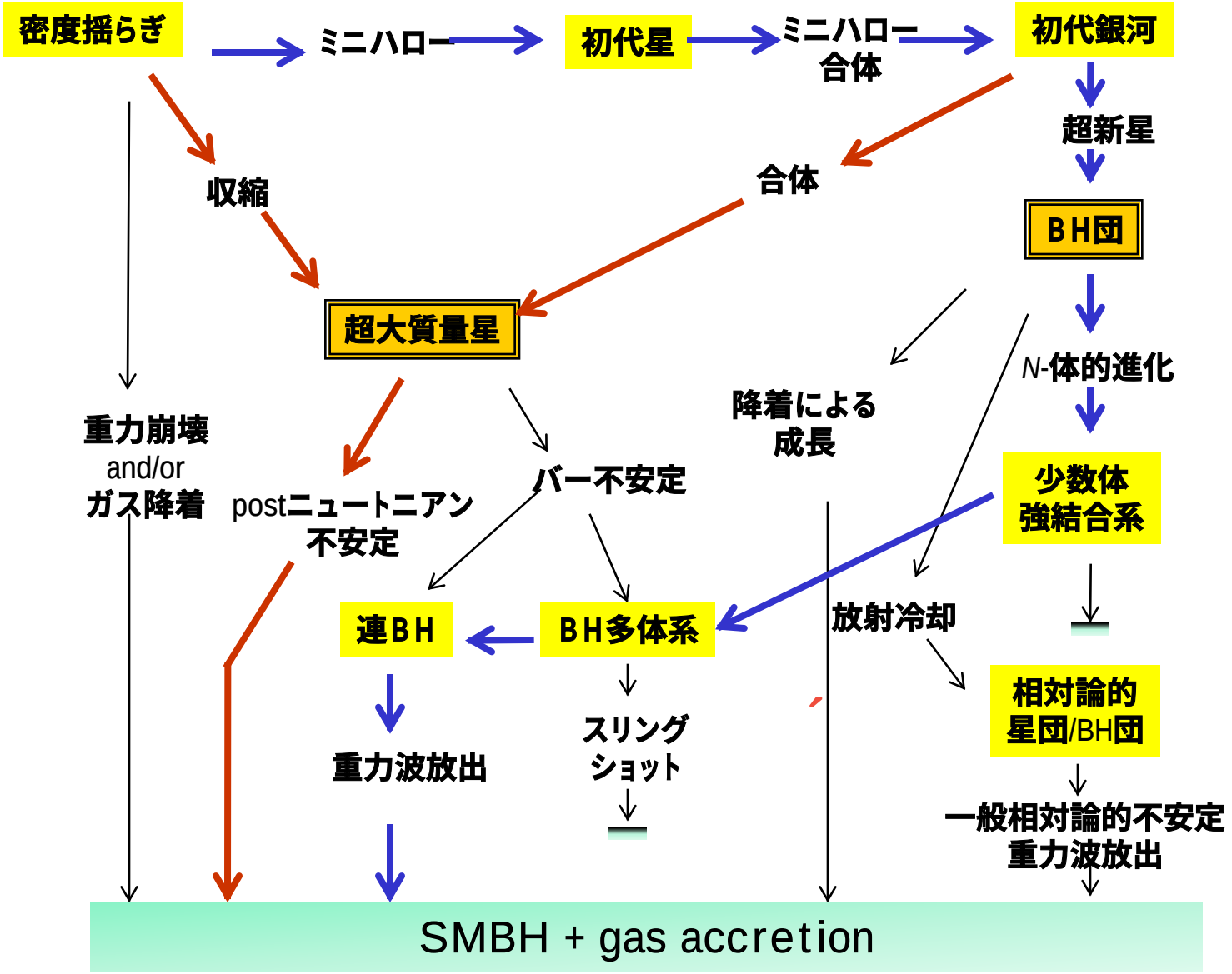

by MU (2014)

QSO Luminosity Functionからの制限
Soltan's Argument (1982)

Integration of QSO LF

$W_{BH}(QSO) \approx 1.8 \times 10^{-6}$

Yu & Tremaine 2002, MNRAS, 335, 965

$W_{BH}(QSO) \approx (2.4 - 4.8) \times 10^{-6}$

Marconi et al. 2004, MNRAS, 351, 169

SMBH-bulge mass relation at z=0

$W_{BH}(bulge) \approx 2.1 \times 10^{-6}$

ß

QSO BHの最終フェーズはガスアクリーションで太った

Accretion Gas Flows

Machida et al. 2004

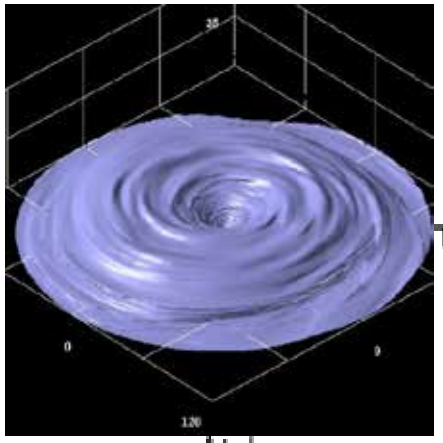

Ohsuga et al. 2005

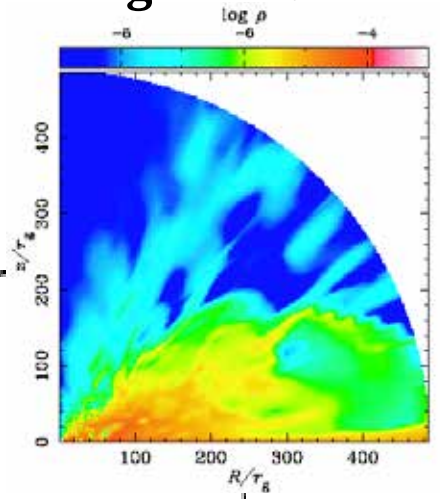

1pc ® BH

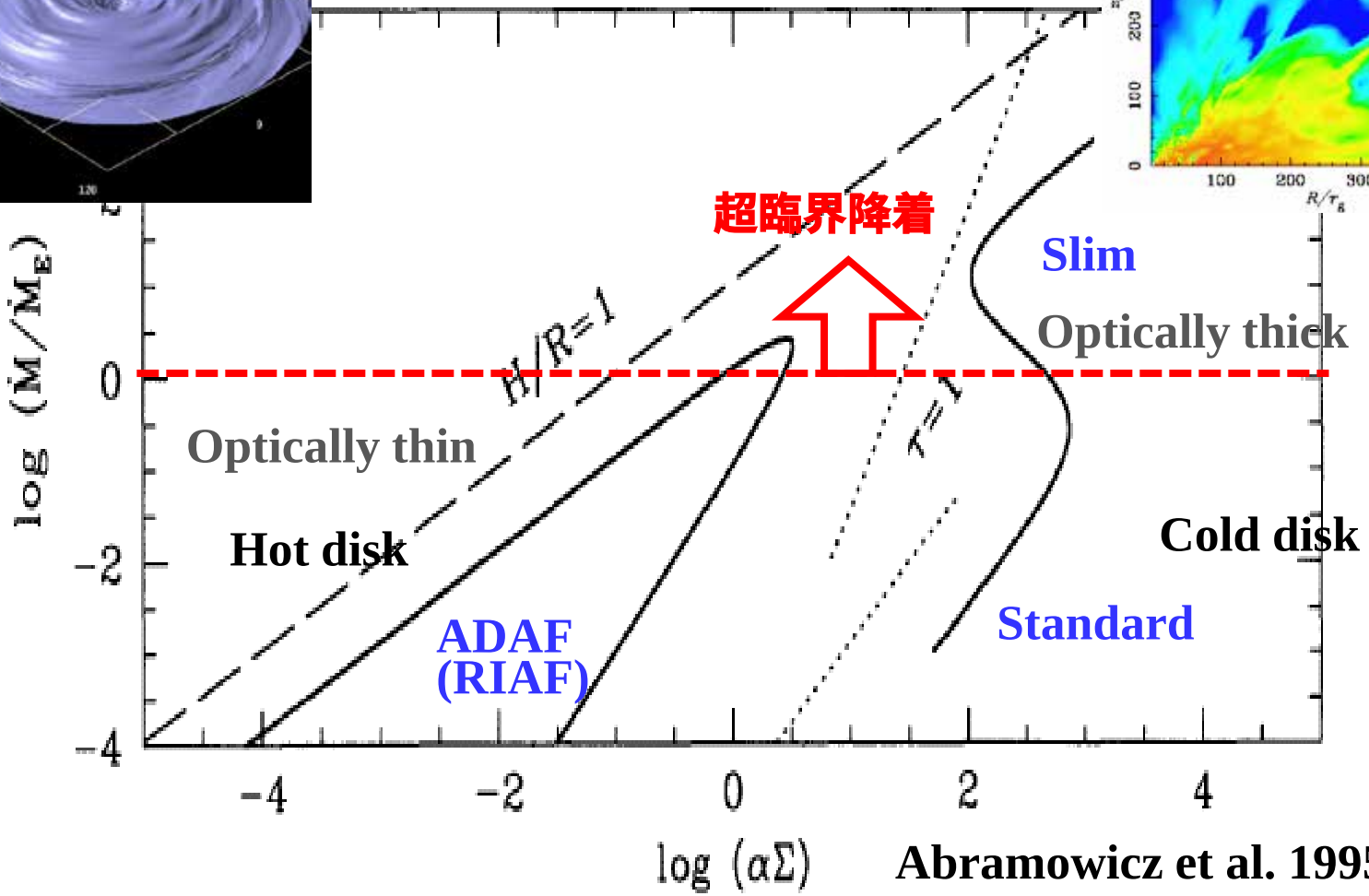

Abramowicz et al. 1995

Accretion Flows

$$L = \eta \dot{M} c^2, \quad L_E = \frac{4\pi G c m_p M_{BH}}{\sigma_T} = \eta \dot{M}_E c^2$$

$$t_E \equiv \frac{M}{\dot{M}_E} = 4.5 \times 10^7 \left(\frac{\eta}{0.1}\right) \mathrm{yr}$$

① Sub-Eddington: RIAF (Radiatively Inefficient Accretion Flow)

Eddington ratio $\dot{m}_E \equiv \dfrac{\dot{M}}{\dot{M}_E} = 1 \quad \Rightarrow \quad \eta \approx 0.1 \dfrac{\dot{M}}{\dot{M}_E}$

② Eddington: Standard Disk

$$\dot{m}_E \equiv \frac{\dot{M}}{\dot{M}_E} \approx 1 \quad \Rightarrow \quad \eta \approx 0.1$$

③ Super-Eddington: Slim Disk (Photon trapping)

$$\dot{m}_E \equiv \frac{\dot{M}}{\dot{M}_E} > 1 \quad \Rightarrow \quad \eta \approx 0.1 \left(\frac{\dot{M}}{\dot{M}_E}\right)^{-1/2}$$

z=7.085 QSO

Mortlock et al. 2011, nature, 474, 616

$L = 6.3' 10^{13} L_{\odot}$, $M_{BH} = 2' 10^{9} M_{\odot}$

Eddigton Ratio $n_E = 1.2$ (Super-Eddigton Accretion)

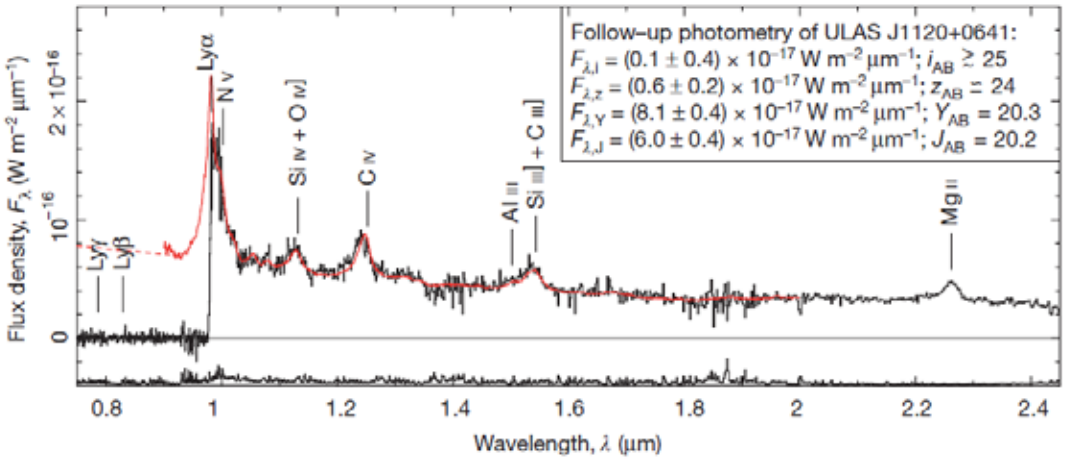

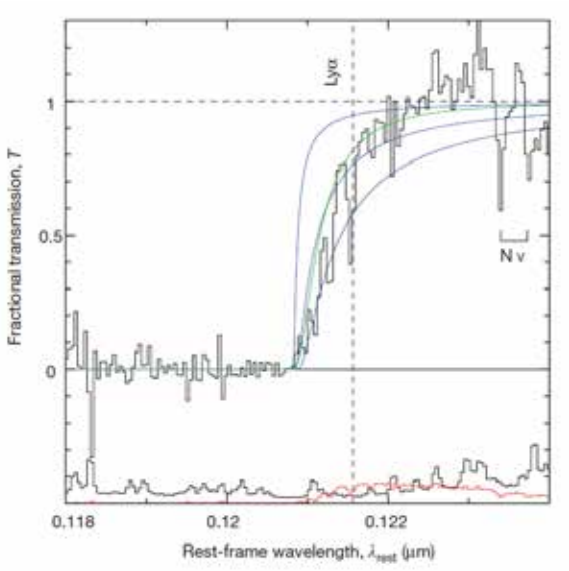

Figure 4 | Rest-frame transmission profile of ULAS J1120+0641 in the region of the Lyα emission line, compared to several damping profiles. The transmission profile of ULAS J1120+0641, obtained by dividing the spectrum by the SDSS composite shown in Fig. 1, is shown in black. The random error spectrum is plotted below the data, also in black. The positive residuals near 0.1230 μm in the transmission profile suggest that the Lyα emission line of ULAS J1120+0641 is actually stronger than average, in which case the absorption would be greater than illustrated. The dispersion in the Lyα equivalent width at a fixed C IV equivalent width of 13% quantifies the uncertainty in the Lyα strength; this systematic uncertainty in the transmission profile is shown in red. The blue curves show the Lyα damping wing of the intergalactic medium for neutral fractions of (from top to bottom) $f_{H\,I} = 0.1$, $f_{H\,I} = 0.5$ and $f_{H\,I} = 1.0$, assuming a sharp ionization front 2.2 Mpc in front of the quasar. The green curve shows the absorption profile of a damped Lyα absorber of column density $N_{H\,I} = 4 \times 10^{20}$ cm^{-2} located 2.6 Mpc in front of the quasar. These curves assume that the ionized zone itself is completely transparent; a more realistic model of the H I distribution around the quasar might be sufficient to discriminate between these two models[25,27]. The wavelength of the Lyα transition is shown as a dashed line; also marked is the N V doublet of the associated absorber referred to in the text.

z=6.30 QSO

Xue-BingWu et al. 2015, nature, 518, 512

$$L=4.29\acute{}\ 10^{14}L_{\odot}\ ,\ M_{\rm BH}=1.2\acute{}\ 10^{10}M_{\odot}$$

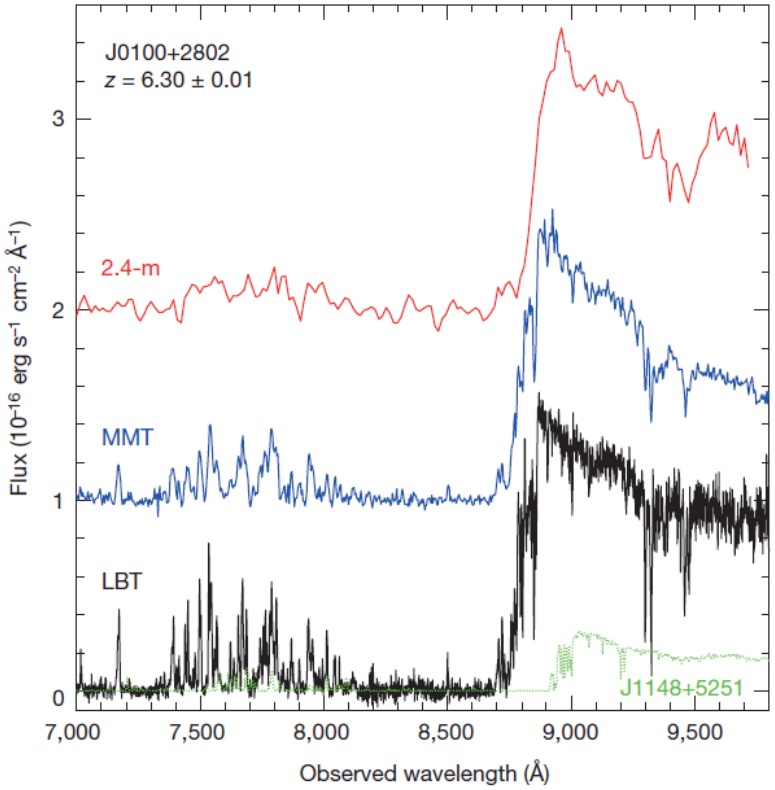

Figure 1 | The optical spectra of J0100+2802. From top to bottom, spectra taken with the Lijiang 2.4-m telescope, the MMT and the LBT (in red, blue and black colours), respectively. For clarity, two spectra are offset upward by one and two vertical units. Although the spectral resolution varies from very low to medium, in all spectra the Lyα emission line, with a rest-frame wavelength of 1,216 Å, is redshifted to around 8,900 Å, giving a redshift of 6.30. J0100+2802 is a weak-line quasar with continuum luminosity about four times higher than that of SDSS J1148+5251 (in green on the same flux scale)[1], which was previously the most luminous high-redshift quasar known at $z = 6.42$.

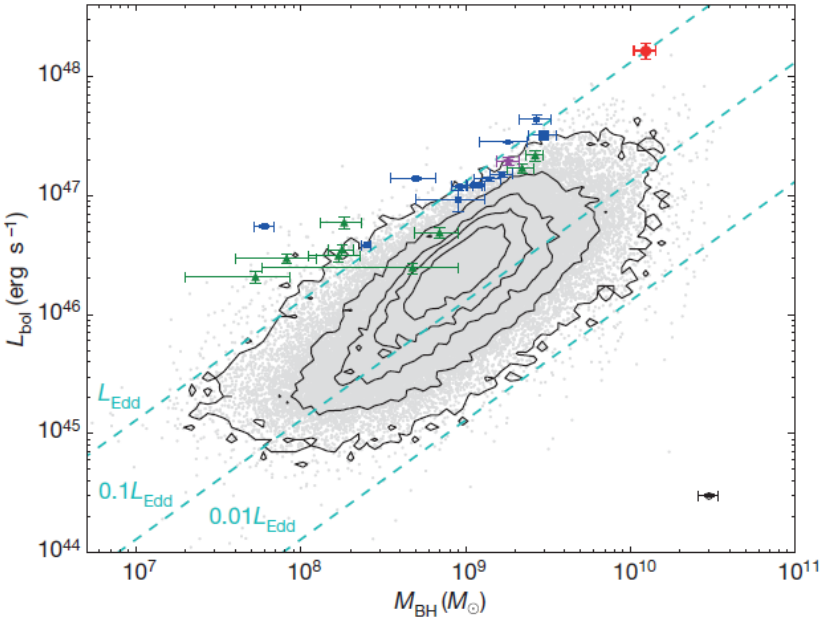

Figure 4 | Distribution of quasar bolometric luminosities, $L_{\rm bol}$, and black-hole masses, $M_{\rm BH}$, estimated from the Mg II lines. The red circle at top right represents J0100+2802. The small blue squares denote SDSS high-redshift quasars[2,10,12], and the large blue square represents J1148+5251. The green triangles denote CFHQS high-redshift quasars[11,12]. The purple star denotes ULAS J1120+0641 at $z = 7.085$ (ref. 6). Black contours (which indicate 1σ to 5σ significance from inner to outer) and grey dots denote SDSS low-redshift quasars[21] (with broad absorption line quasars excluded). Error bars represent the 1σ standard deviation, and the mean error bar for low-redshift quasars is presented in the bottom-right corner. The dashed lines denote the luminosity in different fractions of the Eddington luminosity, $L_{\rm Edd}$. Note that the black-hole mass and bolometric luminosity are calculated using the same method and the same cosmology model as in the present Letter, and the systematic uncertainties (not included in the error bars) of virial black-hole masses could be up to a factor of three[27].

Eddington Growth of z=7.085 QSO SMBH

$$M_{BH}(t) = M_0 \exp\left(\frac{t}{t_E}\right), \quad t_E \equiv \frac{M}{\dot{M}_E} = 4.5 \times 10^7 \left(\frac{\eta}{0.1}\right) \mathrm{yr}$$

$$z_{PopIII} = 20 \; (t = 1.83 \times 10^8 \mathrm{yr}), \; M_0 = 30 M_e$$

$$z_{QSO} = 7.085 \; (t = 7.83 \times 10^8 \mathrm{yr}), \; M_{BH} = 2 \times 10^9 M_e$$

Eddington ratio $\eta_E = 1.4$

Eddington Growth of z=6.30 QSO SMBH

Eddington ratio $\eta_E = 1.3$

But, **一定の超臨界降着を続けることは無理** (Milosavljevic+2009a,b)

Eddington Ratio of QSOs

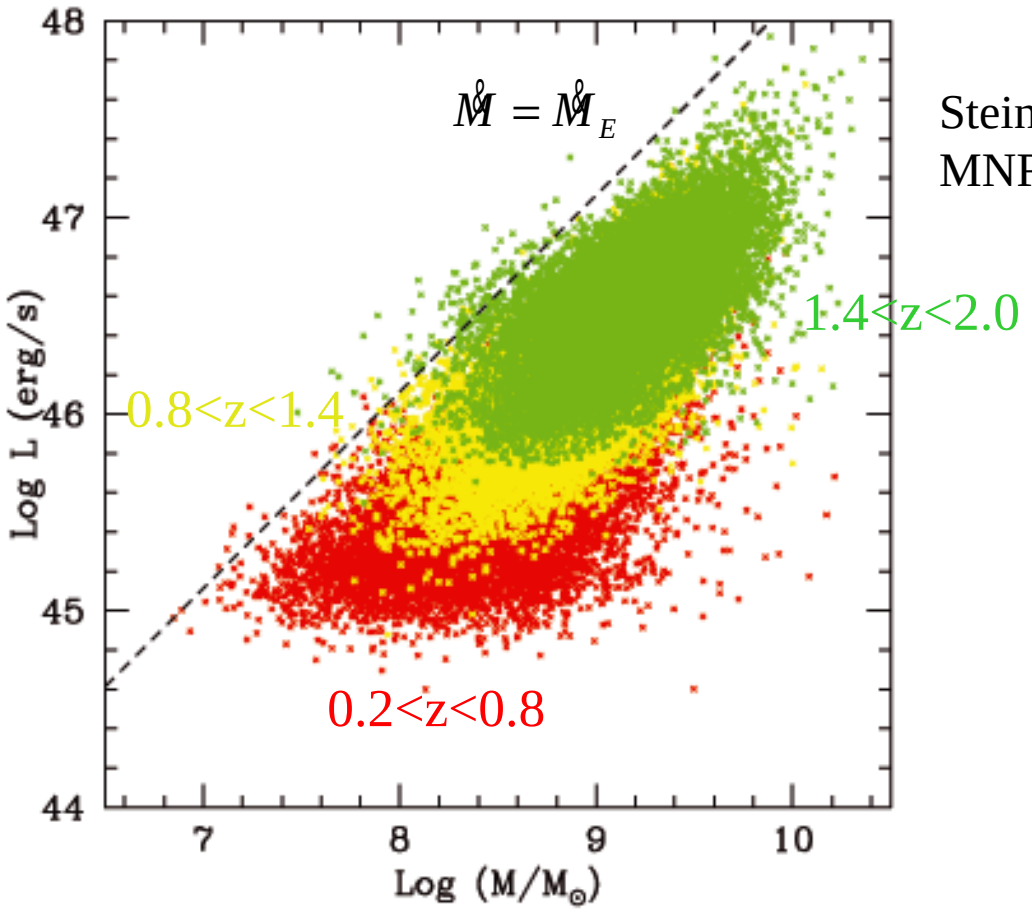

Steinhardt & Elvis 2010, MNRAS, **402,** 2637

Figure 1. The quasar locus in the mass–luminosity plane for all quasars from $0.2 < z < 2.0$, using virial masses estimated by Shen et al. (2008) with Hβ and Mg II lines and bolometric luminosities using the techniques of Richards et al. (2006) The dashed line is drawn at the Eddington luminosity as a function of mass. The colour indicates whether the quasar is at $0.2 < z < 0.8$ (red), $0.8 < z < 1.4$ (yellow) or $1.4 < z < 2.0$ (green).

Growth of Massive BHs

Greene 2012

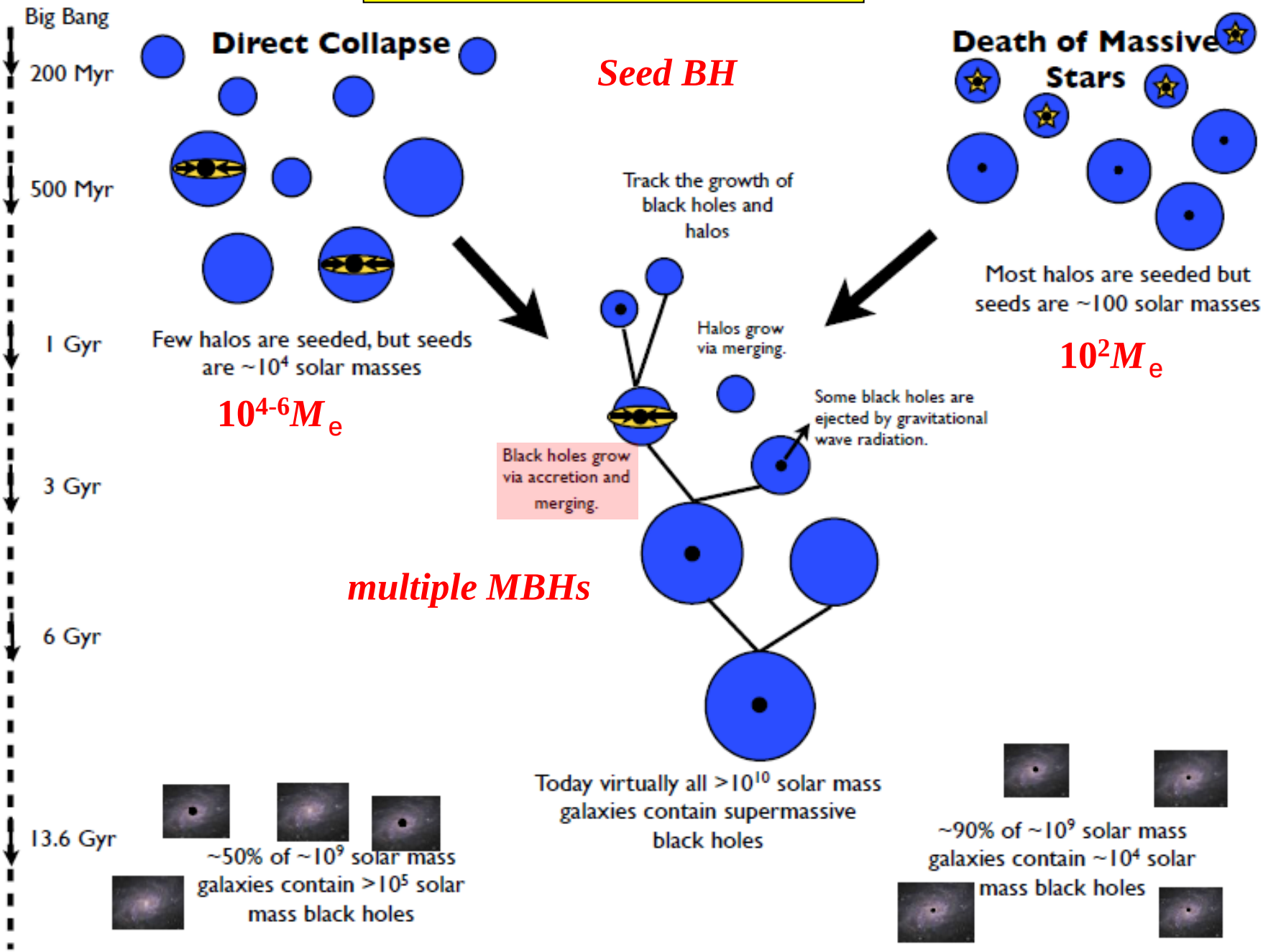

Direct Collapse to Massive Black Holes
超大質量星形成

Suppression of H2 cooling by UV background

Bromm & Loeb 2003, ApJ, 596, 34

$5' 10^6 M_\odot$ MBH binary

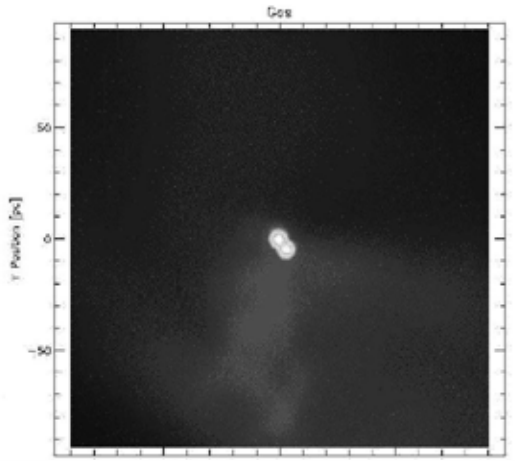

Cold Accretion Shock model

Inayoshi & Omukai 2012, MNRAS, 422, 2539

Warm cloud collapse model

Inayoshi, Omukai, Tasker 2014, MNRASL **445,** L109

$>10^5 M_\odot$ MBH

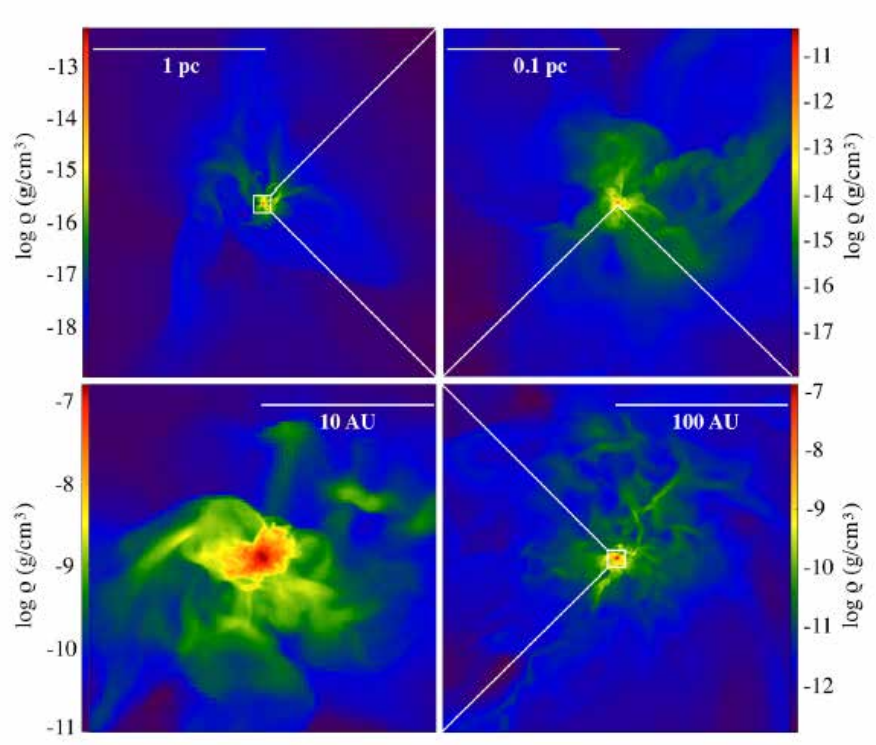

初代星の質量は？

- a few 100$M_\odot$
  (Abel et al. 2000; Bromm et al. 2002; Yoshida et al. 2006)
- bimodal of ~ 1$M_\odot$ & a few 100$M_\odot$ (Nakamura & Umemura 2001)
- several 10$M_\odot$ (Clark et al. 2011)
- about 40$M_\odot$ (Hosokawa et al. 2011)
- a few ~ 10$M_\odot$ (Greif et al. 2011)

Runaway

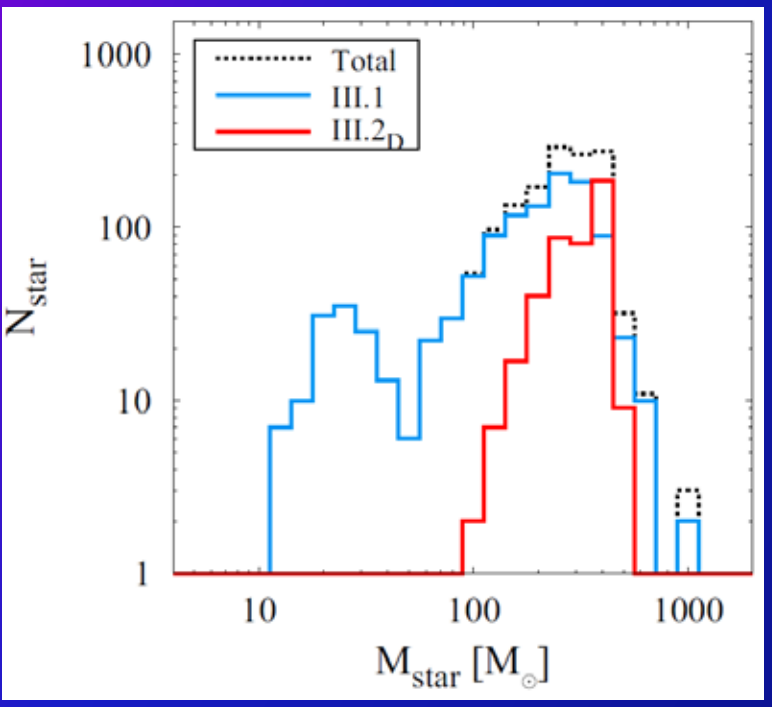

Hirano et al. MNRAS **448,** 568 (2015)

Accretion

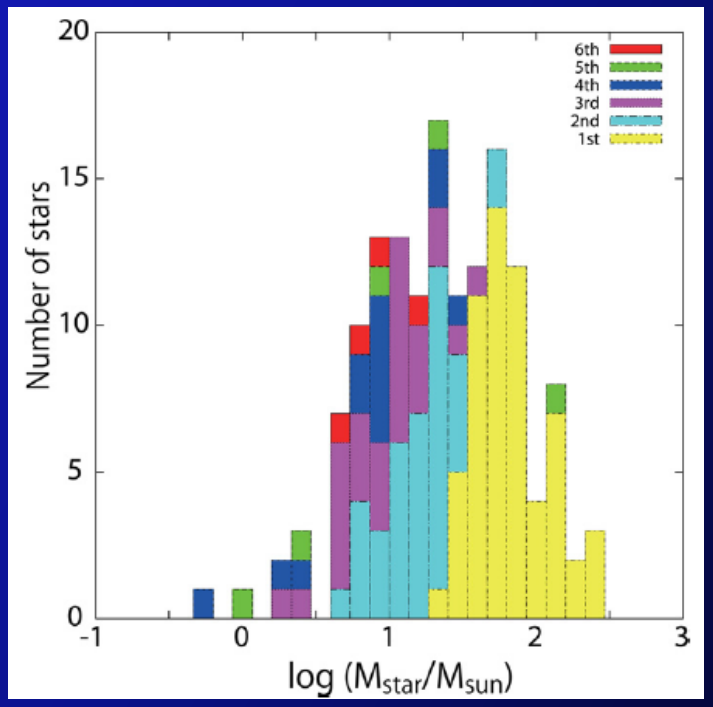

Susa, et al. ApJ, **792**, 32 (2014)

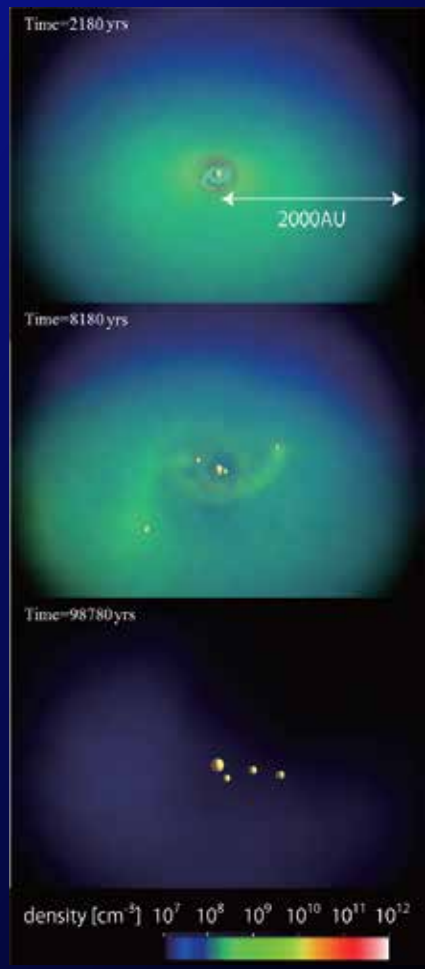

Pop III Star Evolution

Heger & Woosley 2002, ApJ, 567, 532

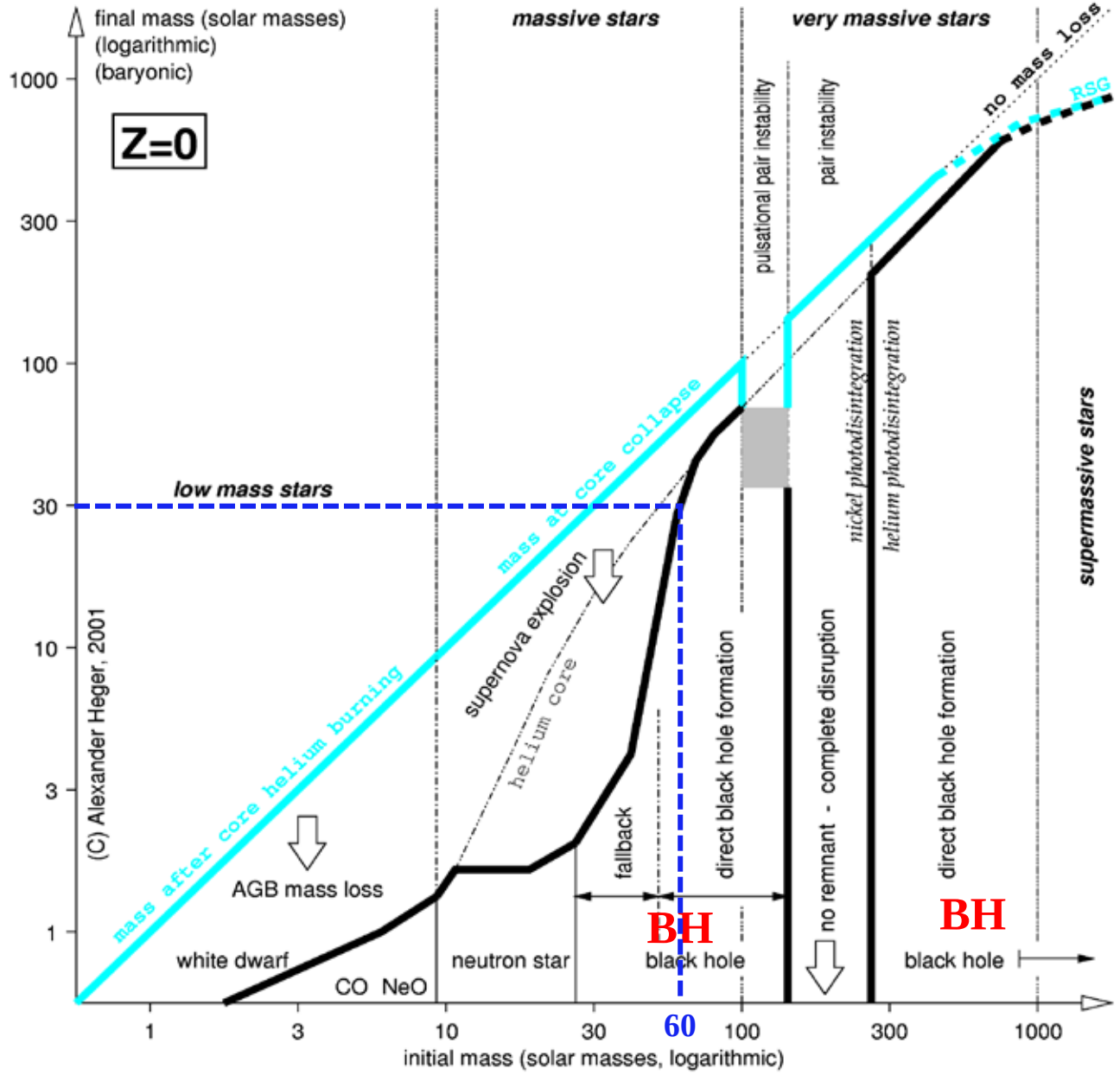

Pop III Binary Formation

Saigo, Matsumoto, Umemura, 2004, ApJL, 615, L65

EOS (Polytrope)
Nested-Grid

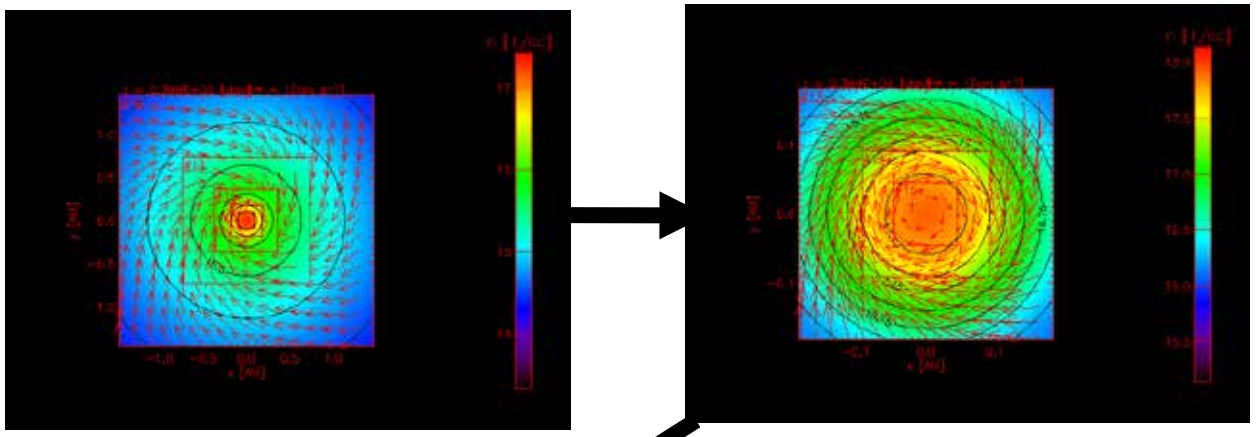

rotationally-supported disk

mass accretion

$\frac{T_{rot}}{|W|} = 0.245$

< 0.27

ring instability

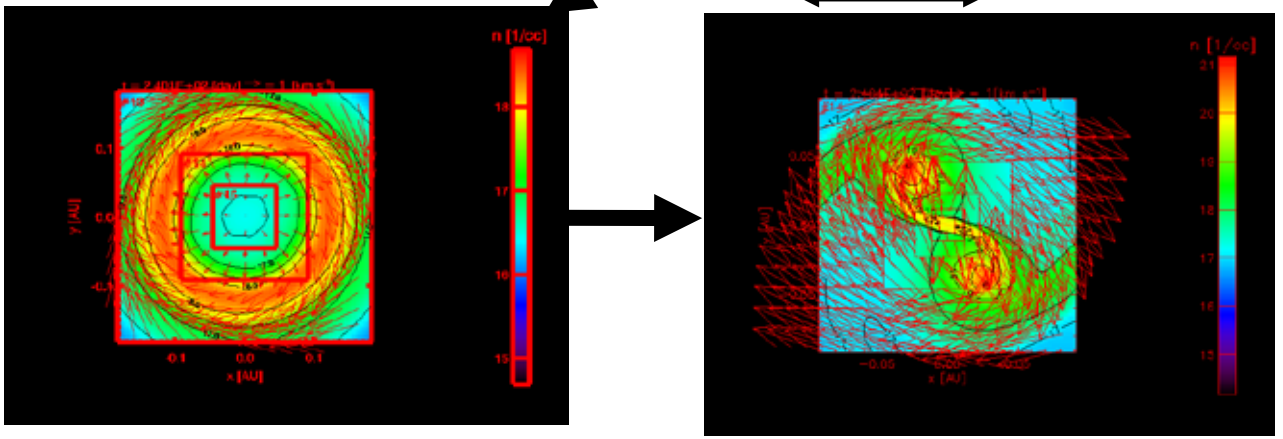

binary Pop III formation

ビリアル定理 $2T + W = 0$ $M \rightarrow aM$ $T + W = (1 - 2a)T$

α=1/2 **なら**binary BH **はできない**

Early Cosmic Merger of Multiple Black Holes

Tagawa, Umemura, Gouda, Yano & Yamai, MNRAS, 451, 2174-2184 (2015)

Post-Newtonian N-body Simulations

Two cases: $30M_e$ BHs, 10^4M_e BHs

$$\frac{d^2\mathbf{r}_i}{dt^2} = \sum_j^{N_{\rm BH}} \left\{ -Gm_j \frac{\mathbf{r}_i - \mathbf{r}_j}{\left|\mathbf{r}_i - \mathbf{r}_j\right|^3} + a_{{\rm PN},ij} \right\} + \boldsymbol{a}_{{\rm DF},i} + \boldsymbol{a}_{{\rm pot},i}$$

初期条件

- **ガス温度** T=1000 K
- **初期ガス質量** $M_{\rm gas}=10^5\,M_{\rm sun}$
- BH**分布**：x-y**平面内に、ランダム**
- BH**速度**：$|\mathbf{v}_{\rm rot}|$　$|\mathbf{v}_{\rm random}|$
- **計算時間**：100 Myr
- **合体条件**：100 $r_{\rm sch}$

4**次の**Hermite**積分法**
(Makino & Aarseth 1992)(η=0.003)

parameter

1. **ガス密度**
2. **初期コンパクト星密度**

Gas dynamical friction

$$\mathbf{a}_{\mathrm{DF},i}^{\mathrm{gas}} = -4\pi G^2 m_i m_{\mathrm{H}} n_{\mathrm{gas}}(r) \frac{\mathbf{v}_i}{{v_i}^3} \times f(\mathcal{M}_i) \qquad (2)$$

$$f(\mathcal{M}_i) = \begin{cases} 0.5\ln\left(\frac{v_i t}{r_{\min}}\right)\left[\mathrm{erf}\left(\frac{\mathcal{M}_i}{\sqrt{2}}\right) - \sqrt{\frac{2}{\pi}}\mathcal{M}_i \exp(-\frac{\mathcal{M}_i^2}{2})\right] \\ (0 \leqslant \mathcal{M}_i \leqslant 0.8) \\ 1.5\ln\left(\frac{v_i t}{r_{\min}}\right)\left[\mathrm{erf}\left(\frac{\mathcal{M}_i}{\sqrt{2}}\right) - \sqrt{\frac{2}{\pi}}\mathcal{M}_i \exp(-\frac{\mathcal{M}_i^2}{2})\right] \\ (0.8 \leqslant \mathcal{M}_i \leqslant \mathcal{M}_{eq}) \\ \frac{1}{2}\ln\left(1 - \frac{1}{\mathcal{M}_i^2}\right) + \ln\left(\frac{v_i t}{r_{\min}}\right), \\ (\mathcal{M}_{eq} \leqslant \mathcal{M}_i) \end{cases}$$

Post-Newtonian

$$\begin{aligned} \boldsymbol{a}_{1\mathrm{PN},ij} = \frac{Gm_j}{r_{ij}^2}\Bigg[\boldsymbol{n}\Bigg[& -{\boldsymbol{v}_i}^2 - 2{\boldsymbol{v}_j}^2 + 4\boldsymbol{v}_i\boldsymbol{v}_j + \frac{3}{2}(\boldsymbol{n}\boldsymbol{v}_j)^2 \\ & + 5\left(\frac{Gm_i}{r_{ij}}\right) + 4\left(\frac{Gm_j}{r_{ij}}\right)\Bigg] \\ & + (\boldsymbol{v}_i - \boldsymbol{v}_j)(4\boldsymbol{n}\boldsymbol{v}_i - 3\boldsymbol{n}\boldsymbol{v}_j)\Bigg], \end{aligned}$$

1PN, 2PN **近日点移動**
2.5 PN=**重力波**

$$\begin{aligned} \boldsymbol{a}_{2\mathrm{PN},ij} = \frac{Gm_j}{r_{ij}^2}\Bigg[\boldsymbol{n}\Bigg[& -2{\boldsymbol{v}_j}^4 + 4{\boldsymbol{v}_j}^2(\boldsymbol{v}_i\boldsymbol{v}_j) - (\boldsymbol{v}_i\boldsymbol{v}_j)^2 \\ & + \frac{3}{2}{\boldsymbol{v}_i}^2(\boldsymbol{n}\boldsymbol{v}_j)^2 + \frac{9}{2}{\boldsymbol{v}_j}^2(\boldsymbol{n}\boldsymbol{v}_j)^2 - 6(\boldsymbol{v}_i\boldsymbol{v}_j)(\boldsymbol{n}\boldsymbol{v}_j)^2 \\ & - \frac{15}{8}(\boldsymbol{n}\boldsymbol{v}_j)^4 + \left(\frac{Gm_i}{r_{ij}}\right)\Bigg[-\frac{15}{4}{\boldsymbol{v}_i}^2 + \frac{5}{4}{\boldsymbol{v}_j}^2 \\ & - \frac{5}{2}\boldsymbol{v}_i\boldsymbol{v}_j + \frac{39}{2}(\boldsymbol{n}\boldsymbol{v}_i)^2 - 39(\boldsymbol{n}\boldsymbol{v}_i)(\boldsymbol{n}\boldsymbol{v}_j) + \frac{17}{2}(\boldsymbol{n}\boldsymbol{v}_i)^2\Bigg] \\ & + \left(\frac{Gm_j}{r_{ij}}\right)\Big[4{\boldsymbol{v}_j}^2 + 8\boldsymbol{v}_i\boldsymbol{v}_j + 2(\boldsymbol{n}\boldsymbol{v}_i)^2 \\ & - 4(\boldsymbol{n}\boldsymbol{v}_i)(\boldsymbol{n}\boldsymbol{v}_j) - 6(\boldsymbol{n}\boldsymbol{v}_i)^2\Big] + (\boldsymbol{v}_i - \boldsymbol{v}_j)\Bigg[{\boldsymbol{v}_i}^2(\boldsymbol{n}\boldsymbol{v}_j) \\ & + 4{\boldsymbol{v}_j}^2(\boldsymbol{n}\boldsymbol{v}_i) - 5{\boldsymbol{v}_j}^2(\boldsymbol{n}\boldsymbol{v}_2) - 4(\boldsymbol{v}_i\boldsymbol{v}_j)(\boldsymbol{n}\boldsymbol{v}_i) \\ & + 4(\boldsymbol{v}_i\boldsymbol{v}_j)(\boldsymbol{n}\boldsymbol{v}_j) - 6(\boldsymbol{n}\boldsymbol{v}_i)(\boldsymbol{n}\boldsymbol{v}_j)^2 + \frac{9}{2}(\boldsymbol{n}\boldsymbol{v}_j)^3\Bigg] \\ & + \left(\frac{Gm_i}{r_{ij}}\right)\left(-\frac{63}{4}\boldsymbol{n}\boldsymbol{v}_i + \frac{55}{4}\boldsymbol{n}\boldsymbol{v}_j\right) \\ & + \left(\frac{Gm_j}{r_{ij}}\right)(-2\boldsymbol{n}\boldsymbol{v}_i - 2\boldsymbol{n}\boldsymbol{v}_j)\Bigg]\Bigg] \\ & + \frac{G^3 m_j}{r_{ij}^4}\boldsymbol{n}\left[-\frac{57}{4}{m_i}^2 - 9{m_j}^2 - \frac{69}{2}m_i m_j\right], \end{aligned} \qquad (12)$$

$$\begin{aligned} \boldsymbol{a}_{2.5\mathrm{PN},ij} = \frac{4}{5}\frac{G^2 m_i m_j}{r_{ij}^3}\Bigg[(\boldsymbol{v}_i - \boldsymbol{v}_j)\Bigg[& -(\boldsymbol{v}_i - \boldsymbol{v}_j)^2 \\ & + 2\left(\frac{Gm_i}{r_{ij}}\right) - 8\left(\frac{Gm_j}{r_{ij}}\right)\Bigg] + \boldsymbol{n}(\boldsymbol{n}\boldsymbol{v}_i - \boldsymbol{n}\boldsymbol{v}_2) \\ & \left[3(\boldsymbol{v}_i - \boldsymbol{v}_j)^2 - 6\left(\frac{Gm_i}{r_{ij}}\right) + \frac{52}{3}\left(\frac{Gm_j}{r_{ij}}\right)\right]\Bigg], \end{aligned} \qquad (13)$$

Type A Gas drag drives the merger

$$M_{\rm gas} \gtrsim 10^5 \sum M_{\rm BH}$$

力学的摩擦による軌道収縮

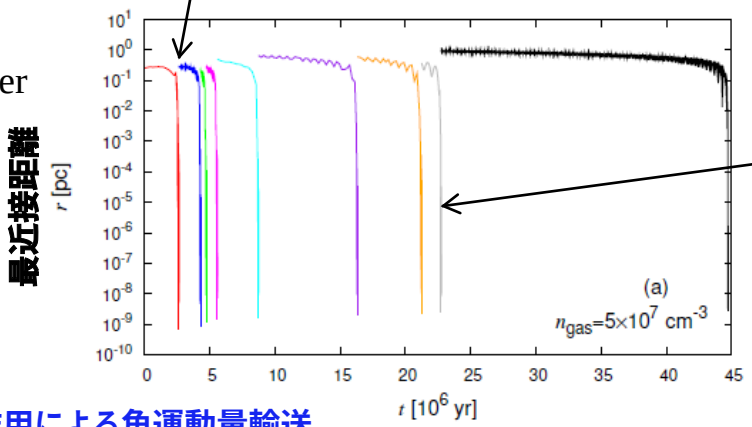

重力波放射による軌道収縮

Type B Three-body reaction and then gas drag drives the merger

$$M_{\rm gas} \lesssim 10^5 \sum M_{\rm BH}$$

3体相互作用による角運動量輸送

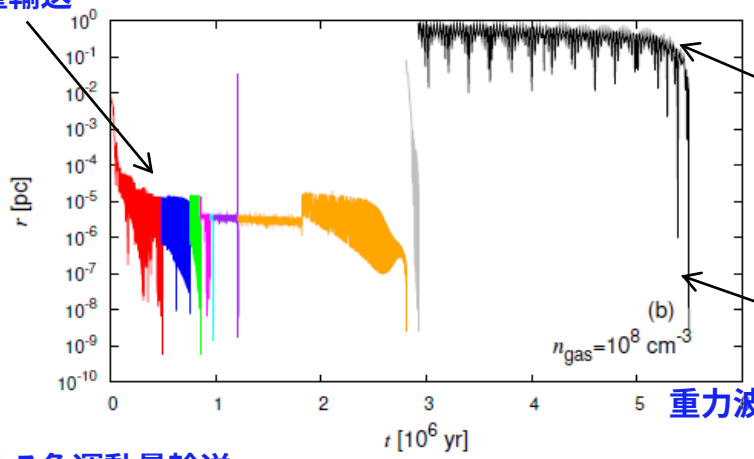

力学的摩擦による軌道収縮

重力波放射による軌道収縮

Type C Three-body reaction drives the merger

$$M_{\rm gas} \ll 10^5 \sum M_{\rm BH}$$

3体相互作用による角運動量輸送

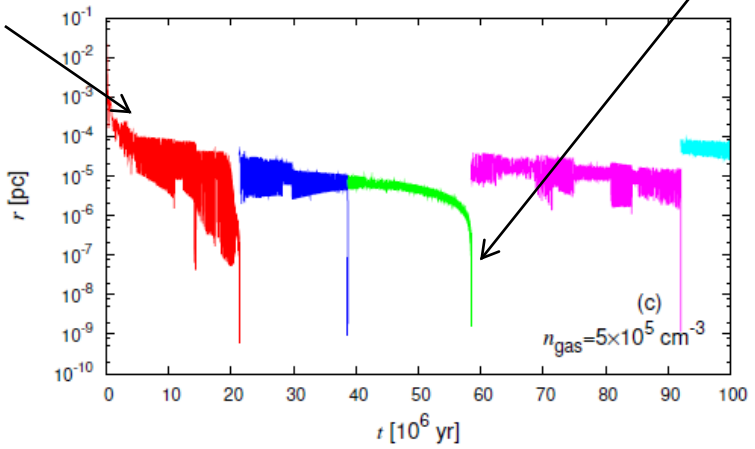

Table 1. The results with $M_{\rm BH} = 30\ M_\odot$ and $N_{\rm BH} = 10$.

$r_{\rm typ}$[pc]	1.0	0.464	0.215	0.1	0.0464	0.0215	0.01
$\rho_{\rm BH}[M_\odot {\rm pc}^{-3}]$	7.2×10^1	7.2×10^2	7.2×10^3	7.2×10^4	7.2×10^5	7.2×10^6	7.2×10^7
$n_{\rm gas}[{\rm cm}^{-3}]$	$N_{\rm m}$ type $t_{\rm fin}$[yr]	$N_{\rm m}$ type $t_{\rm fin}$[yr]	$N_{\rm m}$ type $t_{\rm fin}$[yr]	$N_{\rm m}$ type $t_{\rm fin}$[yr]	$N_{\rm m}$ type $t_{\rm fin}$[yr]	$N_{\rm m}$ type $t_{\rm fin}$[yr]	$N_{\rm m}$ type $t_{\rm fin}$[yr]
10^{12}	0 - 1.0×10^8	5 A 1.0×10^8	**9** A 3.6×10^7	**9** A 4.4×10^6	**9** A 1.7×10^6	**9** A 7.0×10^5	**9** B 4.3×10^5
10^{11}	2 A 1.0×10^8	8 A 1.0×10^8	**9** A 1.3×10^7	**9** A 1.8×10^5	**9** A 1.8×10^5	**9** A 2.3×10^4	**9** B 2.8×10^4
10^{10}	5 A 1.0×10^8	**9** A 4.5×10^7	**9** A 5.1×10^6	**9** A 5.9×10^5	**9** A 7.4×10^4	**9** B 6.3×10^4	**9** B 1.7×10^5
5×10^9	5 A 1.0×10^8	**9** A 2.9×10^7	**9** A 3.1×10^6	**9** A 4.5×10^5	**9** B 1.6×10^5	**9** B 3.4×10^5	**9** B 7.7×10^4
10^9	8 A 1.0×10^8	**9** A 2.4×10^7	**9** A 3.5×10^6	**9** B 2.6×10^5	**9** B 4.3×10^5	**9** B 3.5×10^5	**9** B 3.0×10^5
5×10^8	8 A 1.0×10^8	**9** A 1.2×10^7	**9** A 1.3×10^6	**9** B 6.5×10^5	**9** B 4.3×10^5	**9** B 5.5×10^5	**9** B 5.1×10^5
10^8	**9** A 3.0×10^7	**9** A 5.1×10^6	**9** B 4.0×10^6	**9** B 5.5×10^6	**9** B 3.6×10^6	**9** B 4.2×10^6	**9** B 1.2×10^7
5×10^7	**9** A 4.5×10^7	**9** B 3.7×10^6	**9** B 2.2×10^7	**9** B 3.2×10^7	**9** B 1.3×10^7	**9** B 4.7×10^6	**9** B 3.6×10^6
10^7	**9** B 3.8×10^7	**9** B 2.3×10^7	**9** B 1.7×10^7	**9** B 3.3×10^7	**9** B 1.8×10^7	**9** B 2.9×10^7	**9** B 1.7×10^7
5×10^6	**9** B 4.2×10^7	**9** B 3.9×10^7	**9** B 4.2×10^7	**9** B 4.7×10^7	**9** B 6.3×10^7	**9** B 3.5×10^7	**9** B 3.1×10^7
10^6	6 B 1.0×10^8	6 B 1.0×10^8	8 B 1.0×10^8	6 C 1.0×10^8	8 C 1.0×10^8	6 C 1.0×10^8	6 C 1.0×10^8
5×10^5	2 C 1.0×10^8	6 C 1.0×10^8	6 C 1.0×10^8	4 C 1.0×10^8	5 C 1.0×10^8	3 C 1.0×10^8	4 C 1.0×10^8
10^5	0 - 1.0×10^8	0 - 1.0×10^8	1 C 1.0×10^8	0 - 1.0×10^8	1 C 1.0×10^8	2 C 1.0×10^8	0 - 1.0×10^8
10^4	0 - 1.0×10^8	0 - 1.0×10^8	0 - 1.0×10^8	1 C 1.0×10^8	0 - 1.0×10^8	0 - 1.0×10^8	0 - 1.0×10^8

初代天体領域

Table 2. The results with $M_{\rm BH} = 10^4\ M_\odot$ and $N_{\rm BH} = 10$.

$r_{\rm typ}$[pc]	10.0	4.64	2.15	1.0	0.464	0.215	0.1
$\rho_{\rm BH}[M_\odot {\rm pc}^{-3}]$	2.4×10^1	2.4×10^2	2.4×10^3	2.4×10^4	2.4×10^5	2.4×10^6	2.4×10^7
$n_{\rm gas}[{\rm cm}^{-3}]$	$N_{\rm m}$ type $t_{\rm fin}$[yr]	$N_{\rm m}$ type $t_{\rm fin}$[yr]	$N_{\rm m}$ type $t_{\rm fin}$[yr]	$N_{\rm m}$ type $t_{\rm fin}$[yr]	$N_{\rm m}$ type $t_{\rm fin}$[yr]	$N_{\rm m}$ type $t_{\rm fin}$[yr]	$N_{\rm m}$ type $t_{\rm fin}$[yr]
10^{12}	0 - 1.0×10^8	4 A $\times10^{10}$	7 A $\times10^{10}$	**9** A 1.3×10^7	**9** A 1.5×10^6	**9** A 1.7×10^5	**9** A 2.2×10^4
10^{11}	0 - 1.0×10^8	5 A 1.0×10^8	**9** A 4.6×10^7	**9** A 5.0×10^6	**9** A 5.8×10^5	**9** A 7.2×10^4	**9** B 1.6×10^4
10^{10}	4 A 1.0×10^8	8 A 1.0×10^8	**9** A 1.7×10^7	**9** A 2.0×10^6	**9** A 2.5×10^5	**9** A 9.3×10^4	**9** B 4.1×10^4
10^9	5 A 1.0×10^8	**9** A 5.8×10^7	**9** A 7.0×10^6	**9** A 9.6×10^5	**9** B 7.6×10^5	**9** B 9.0×10^5	**9** B 2.4×10^6
5×10^8	5 A 1.0×10^8	**9** A 5.0×10^7	**9** A 1.0×10^7	**9** B 1.5×10^6	**9** B 9.5×10^5	**9** B 7.6×10^5	**9** B 6.7×10^5
10^8	7 A 1.0×10^8	**9** A 2.5×10^7	**9** B 3.7×10^6	**9** B 8.3×10^6	**9** B 4.9×10^6	**9** B 5.6×10^6	**9** B 7.9×10^6
5×10^7	**9** A 7.3×10^7	**9** A 2.0×10^7	**9** B 1.3×10^7	**9** B 7.1×10^6	**9** B 1.2×10^7	**9** B 3.5×10^6	**9** B 9.4×10^6
10^7	**9** B 7.7×10^7	**9** B 3.5×10^7	**9** B 9.3×10^7	**9** B 6.0×10^7	**9** B 3.3×10^7	**9** B 3.6×10^7	**9** B 4.1×10^7
5×10^6	8 B 1.0×10^8	**9** B 8.3×10^7	**9** B 3.9×10^7	**9** B 8.5×10^7	**9** B 4.6×10^7	**9** B 4.8×10^7	**9** B 7.9×10^7
10^6	5 B 1.0×10^8	7 B 1.0×10^8	4 B 1.0×10^8	**9** B 6.5×10^7	5 C 1.0×10^8	5 C 1.0×10^8	6 C 1.0×10^8
5×10^5	3 B 1.0×10^8	3 C 1.0×10^8	3 C 1.0×10^8	3 C 1.0×10^8	6 C 1.0×10^8	4 C 1.0×10^8	4 C 1.0×10^8
10^5	0 - 1.0×10^8	0 - 1.0×10^8	0 - 1.0×10^8	0 - 1.0×10^8	0 - 1.0×10^8	1 C 1.0×10^8	0 - 1.0×10^8
5×10^4	0 - 1.0×10^8	0 - 1.0×10^8	1 C 1.0×10^8	0 - 1.0×10^8	1 C 1.0×10^8	1 C 1.0×10^8	1 C 1.0×10^8
10^4	0 - 1.0×10^8	0 - 1.0×10^8	0 - 1.0×10^8	0 - 1.0×10^8	0 - 1.0×10^8	0 - 1.0×10^8	1 C 1.0×10^8

質量降着
Bondi-Hoyle-Littleton Accretion

$$\dot{M}_{BHL} = 4\pi r \frac{G^2 M^2}{(v^2 + c_s^2)^{3/2}} \qquad \therefore \; M = \frac{1}{M_0^{-1} - \alpha t}$$

$$t_{\ast} = 1.7 \times 10^9 \,\mathrm{yr} \left(\frac{v}{100\ \mathrm{km\ s^{-1}}}\right)^3 \left(\frac{n}{10^2 \mathrm{cm^{-3}}}\right)^{-1} \left(\frac{M_0}{10^6 M_e}\right)^{-1}$$

$$\dot{M}_{BHL} = 0.6 \times 10^{-3} M_e \,\mathrm{yr} \left(\frac{v}{100\ \mathrm{km\ s^{-1}}}\right)^{-3} \left(\frac{n}{10^2 \mathrm{cm^{-3}}}\right) \left(\frac{M_0}{10^6 M_e}\right)^2$$

$$\dot{M}_E = 2 \times 10^{-2} M_e \,\mathrm{yr}^{-1} \left(\frac{M_0}{10^6 M_e}\right)$$

Mergers of Accreting Stellar Mass Black Holes

(Tagawa, Umemura, et al. 2016 arXiv:1602.08767)

Physical situation

初代星形成の3次元輻射流体計算

(Greif 2011, Susa 2013, Susa et al. 2014)

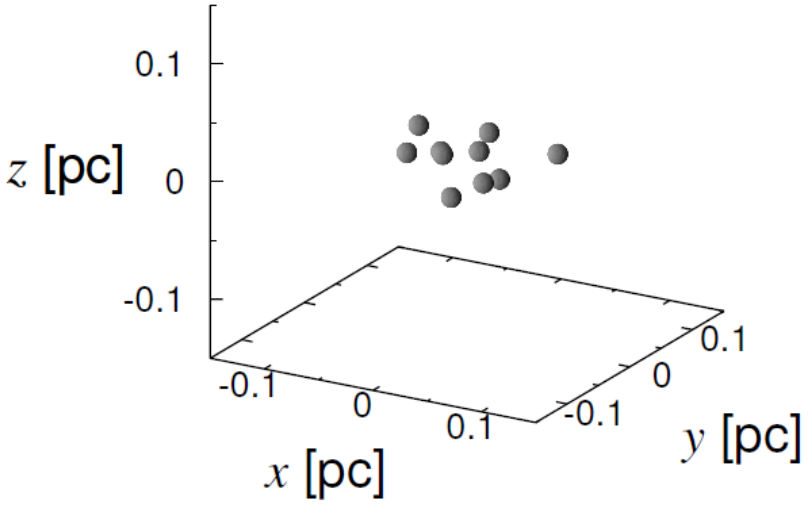

初期条件

- **ガス温度** T=1000 K
- **初期ガス質量** $M_{\rm gas}=10^5\,M_\odot$
- **BH質量** $m_{\rm BH}=30\,M_\odot$
- **BH数** N=10
- **BH分布**：x-y**平面内に、ランダム**
- **BH速度**：$|\mathbf{v}_{\rm rot}|$　$|\mathbf{v}_{\rm random}|$
- **計算時間**：100 Myr
- **合体条件**：100 $r_{\rm sch}$

キーパラメーター

1. **初期ガス密度**$(n_{\rm gas})$
2. **初期BH密度**$(\rho_{\rm BH})$
3. **ガス降着率** $(\mathrm{e}=\dot{m}/\dot{m}_{\rm HL})$

計算手法

- 4次のHermite積分法 (Makino & Aarseth 1992)(η=0.003)
- Post Newtonian近似 (Kupi 2006)で近日点移動と重力波放出
- ガスによる力学的摩擦 (Ostriker 1999)
- Hoyle-Lyttleton降着と輻射圧を考慮した降着率の上限値設定

(Watarai et al. 2000; Hanamoto, Ioroi & Fukue 2001)

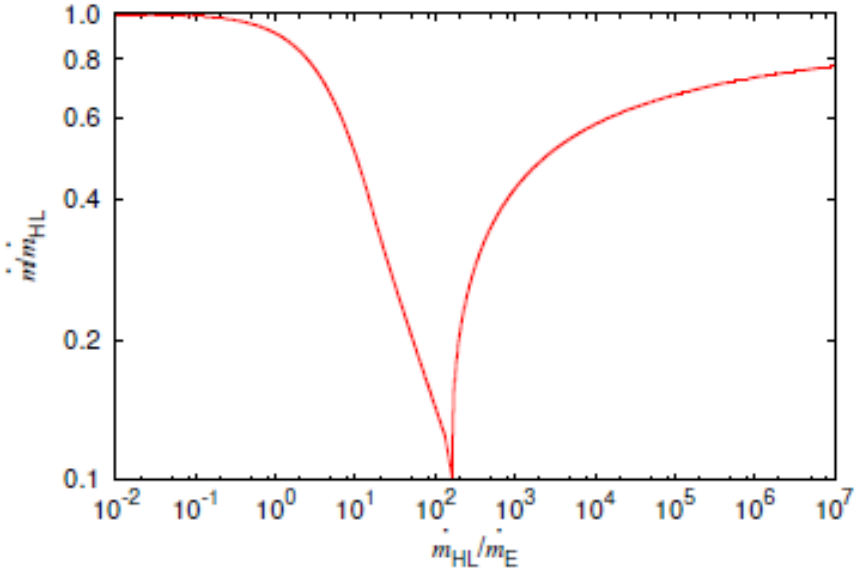

Mergers of 30 $M_\odot$ Black Holes

(Tagawa, Umemura, et al. 2015, MNRAS 451, 2174; 2016 arXiv:1602.08767)

Post-Newtonian N-body Simulations (2.5PN=GW)

Type A
Gas drag-driven merger

$t = 1.6 \times 10^3$ yr
$m_{ac,tot} = 12\ M_{sun}$
$N_{merge} = 4$

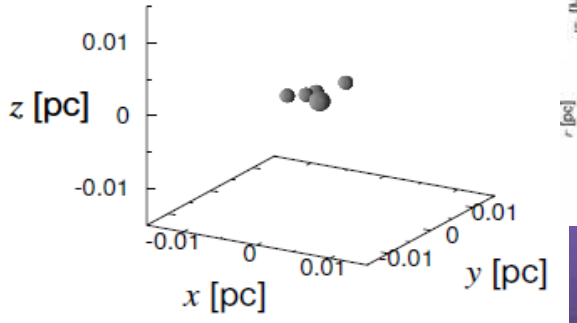

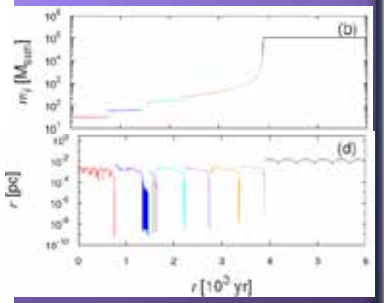

Type B
Interplay-driven merger

$t = 1.5 \times 10^5$ yr
$m_{ac,tot} = 3.7 \times 10^{-2}\ M_{sun}$
$N_{merge} = 6$

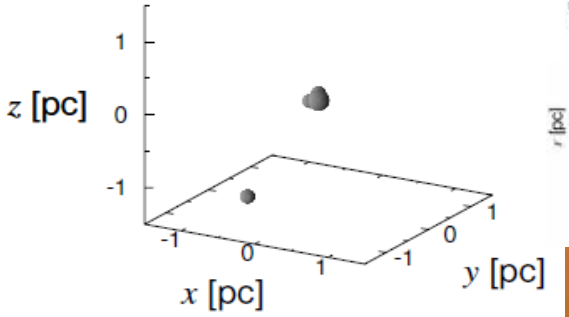

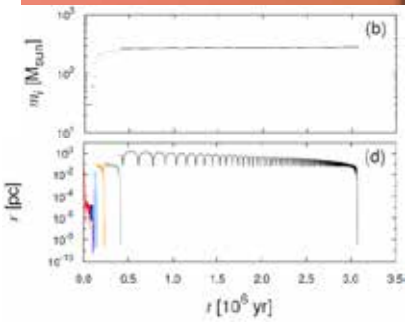

Type C
Three body-driven merger

$t = 2.7 \times 10^7$ yr
$m_{ac,tot} = 6.3 \times 10^{-3}\ M_{sun}$
$N_{merge} = 2$

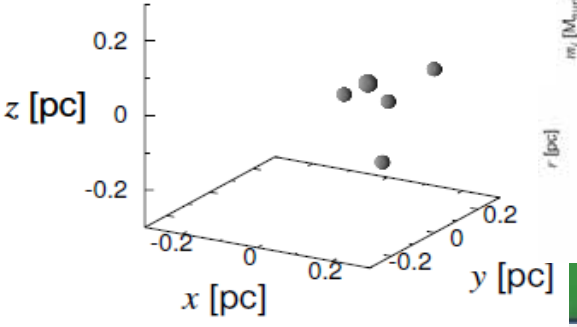

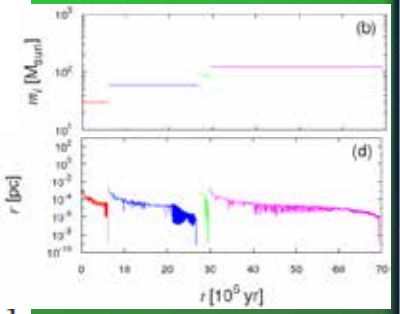

Type D
Accretion-driven merger

$t = 1.9 \times 10^5$ yr
$m_{ac,tot} = 1 \times 10^5\ M_{sun}$
$N_{merge} = 0$

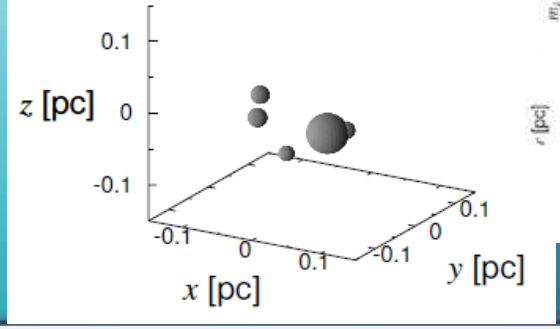

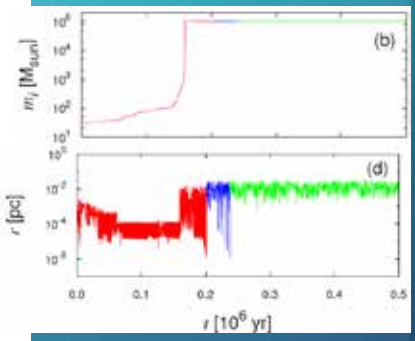

合体条件と質量降着

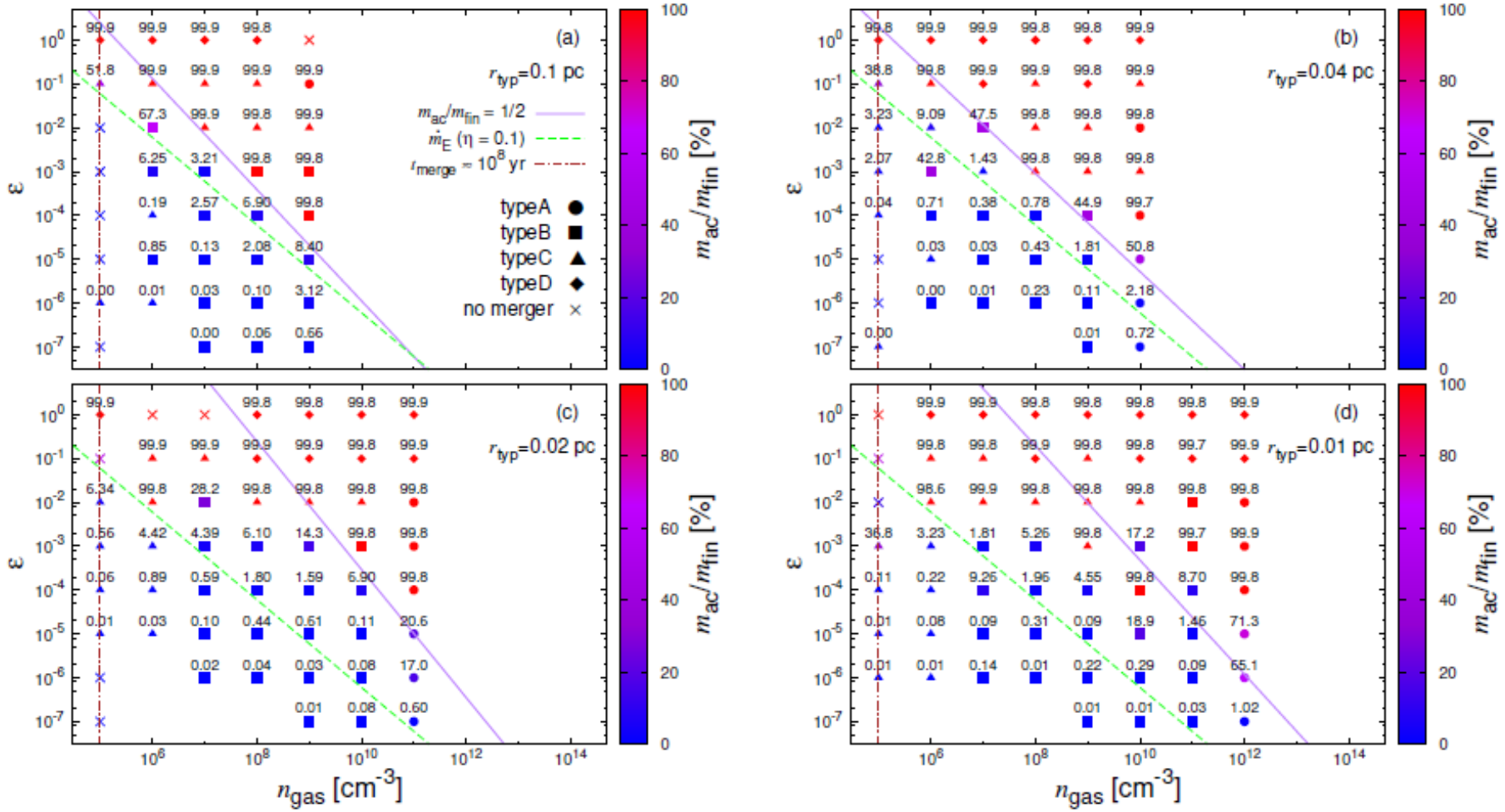

$\dot{M} < 10\dot{M}_E$ なら，大きな降着が起きる前に合体

Super –Eddington でも合体の方が速く起こる

GW150914
LIGO Observation

Abbott et al. 2016a, b, c, d, e, f, g, h, i

a. **Observation of Gravitational Waves from a Binary Black Hole Merger**
b. **Calibration of the Advanced LIGO detectors for the discovery of the binary black-hole merger**
c. **Properties of the binary black hole merger GW150914**
d. **Astrophysical Implications of the Binary Black-Hole Merger GW150914**
e. **GW150914: Implications for the stochastic gravitational-wave background from binary black holes**
f. **Tests of general relativity with GW150914**
g. **Observing gravitational-wave transient GW150914 with minimal assumptions**
h. **The Rate of Binary Black Hole Mergers Inferred from Advanced LIGO Observations Surrounding GW150914**
i. **GW150914: First results from the search for binary black hole coalescence with Advanced LIGO**

VIRGO was being upgraded
GEO 600 was not in observational mode

重力波初検出

Advanced LIGO (Laser Interferometer Gravitational-Wave Observatory), Sep 12, 2015
Hanford, Washington (H1) & Livingston, Louisiana (L1), observatories

Michelson interferometer

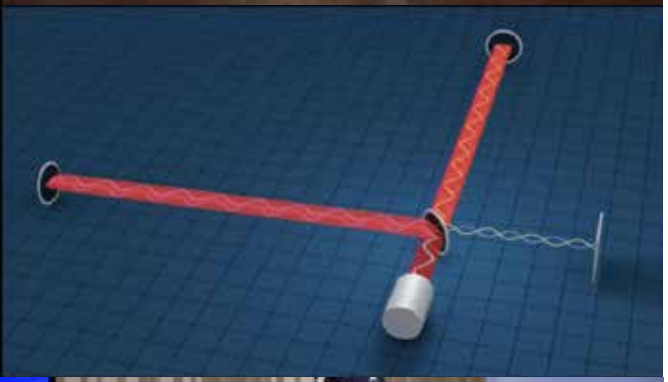

dual-chain, quadruple pendulum（振り子）
suspension systems

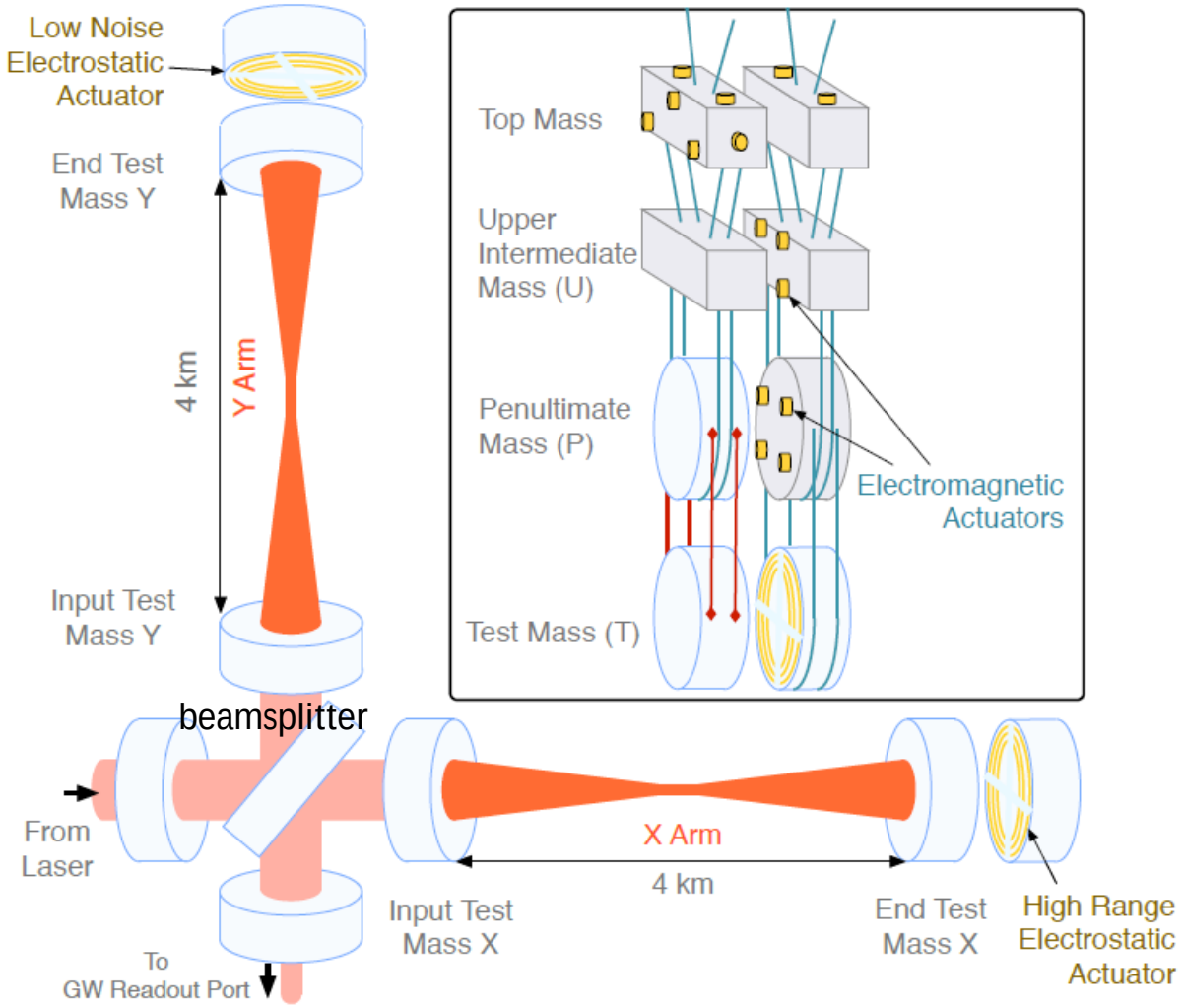

Observations (Results)

Advanced LIGO detected GW on Sep 14, 2015, 09:50:45 UTC

False alarm rate is less than 1/203 000 yr (5.1s)

Merger of a binary composed of 36$M_\odot$ and 29$M_\odot$ BHs (z=0.09)

Luminosity = 3.6×10^{56} erg/s cf. GRB 10^{52} erg/s

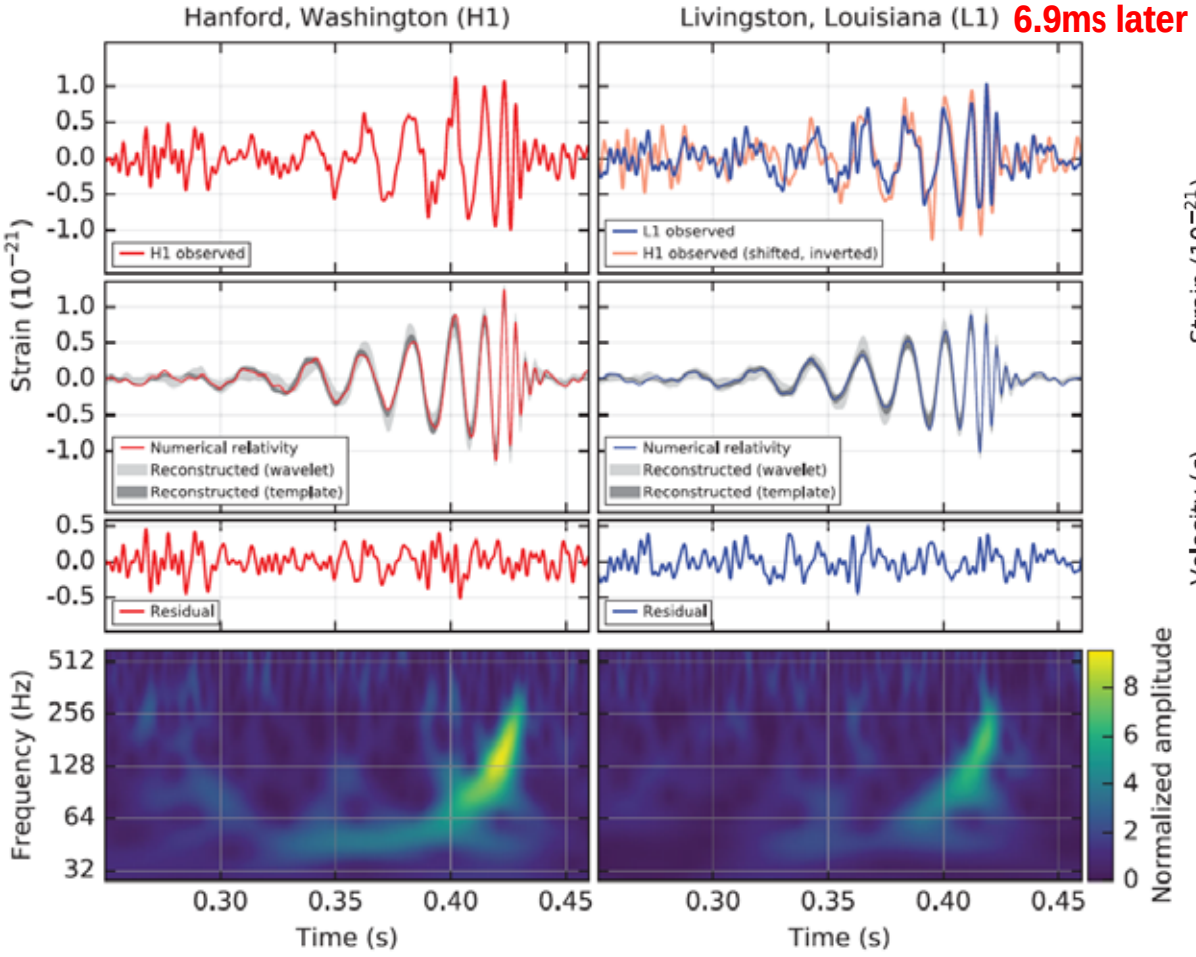

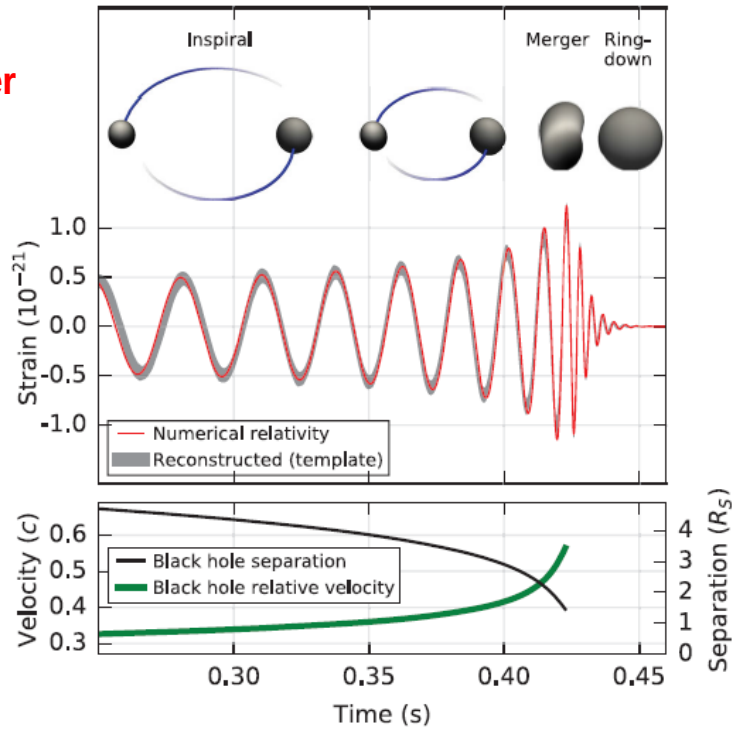

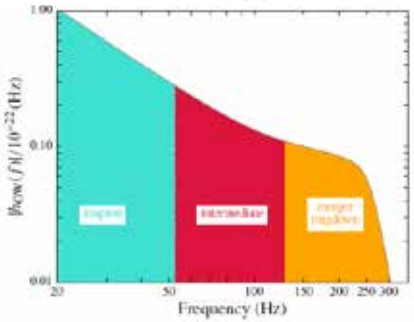

class C1: events with time-frequency morphology of noise transients
class C3: events with frequency that increases with time
class C2: all remaining events

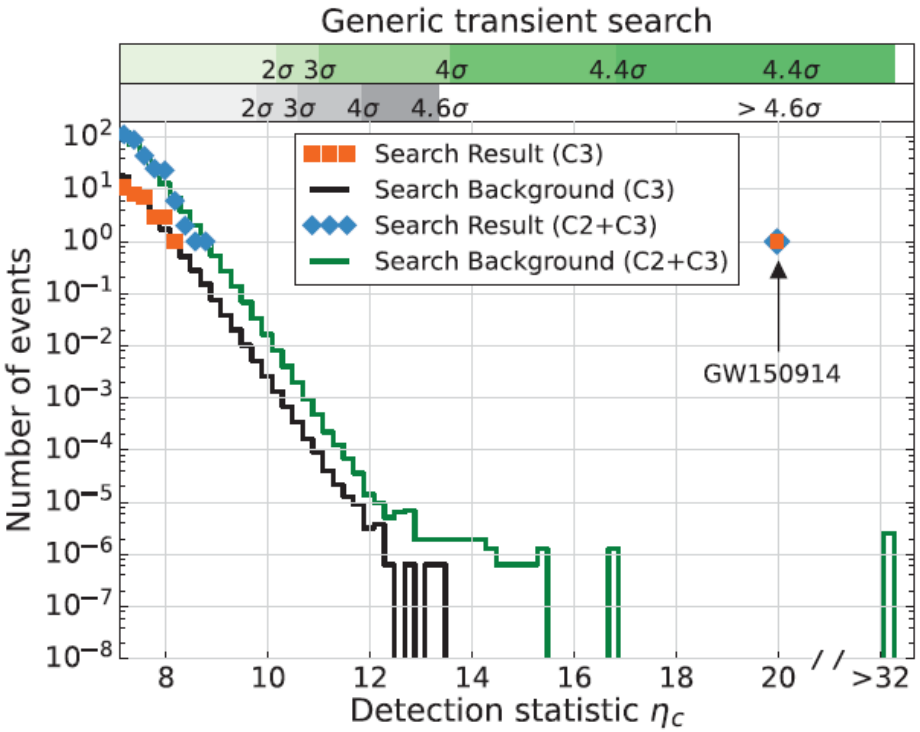

$\eta_c = \sqrt{2E_c/(1 + E_n/E_c)}$, where E_c is the dimensionless coherent signal energy obtained by cross-correlating the two reconstructed waveforms, and E_n is the dimensionless residual noise energy after the reconstructed signal is subtracted from the data. The statistic η_c thus quantifies the SNR of the event and the consistency of the data between the two detectors.

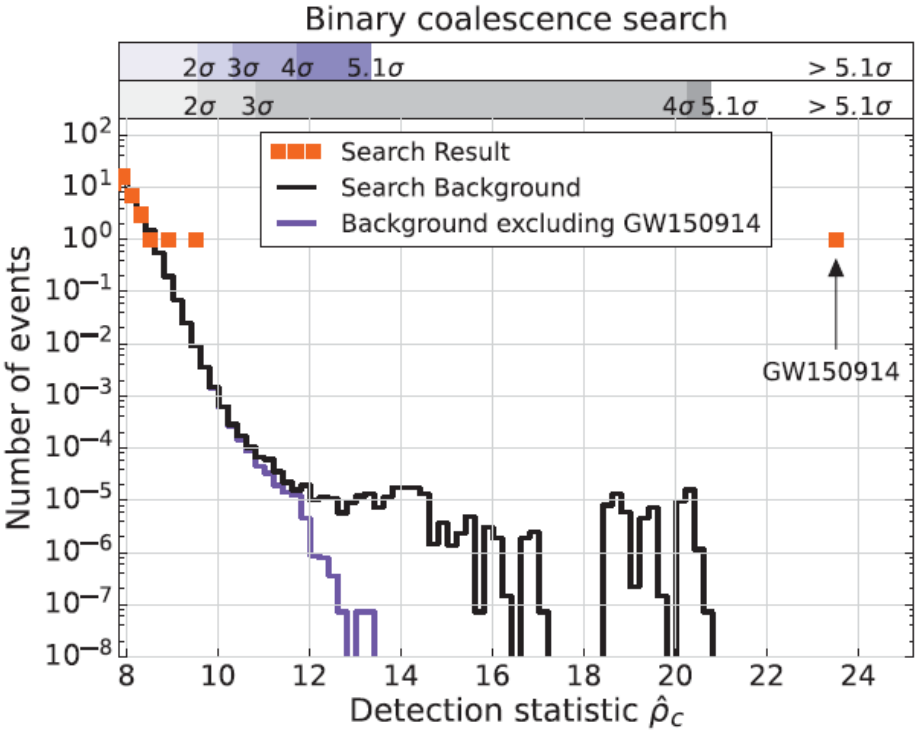

The search calculates the matched-filter signal-to-noise ratio $\rho(t)$ for each template in each detector and identifies maxima of $\rho(t)$ with respect to the time of arrival of the signal [79–81]. For each maximum we calculate a chi-squared statistic χ^2_r to test whether the data in several different frequency bands are consistent with the matching template [82]. Values of χ^2_r near unity indicate that the signal is consistent with a coalescence. If χ^2_r is greater than unity, $\rho(t)$ is reweighted as $\hat{\rho} = \rho/\{[1 + (\chi^2_r)^3]/2\}^{1/6}$ [83,84]. The final step enforces coincidence between detectors by selecting event pairs that occur within a 15-ms window and come from the same template. The 15-ms window is determined by the 10-ms intersite propagation time plus 5 ms for uncertainty in arrival time of weak signals. We rank coincident events based on the quadrature sum $\hat{\rho}_c$ of the $\hat{\rho}$ from both detectors [45].

False alarm rate is less than 1/203 000 yr (5.1s)

Mass Determination

250, 000 template waveforms

$m_1 = 36^{+5}_{-4} M_\odot$ $m_2 = 29^{+4}_{-4} M_\odot$

Primary black hole mass	$36^{+5}_{-4} M_\odot$
Secondary black hole mass	$29^{+4}_{-4} M_\odot$
Final black hole mass	$62^{+4}_{-4} M_\odot$
Final black hole spin	$0.67^{+0.05}_{-0.07}$
Luminosity distance	410^{+160}_{-180} Mpc
Source redshift z	$0.09^{+0.03}_{-0.04}$

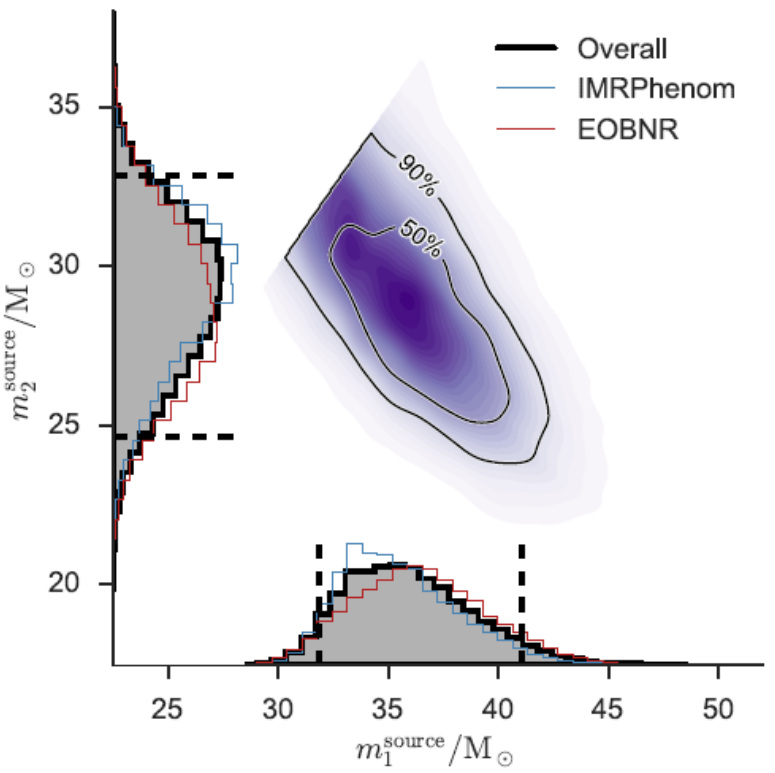

FIG. 1. Posterior PDFs for the source-frame component masses $m_1^{\rm source}$ and $m_2^{\rm source}$, where $m_2^{\rm source} \leq m_1^{\rm source}$. In the 1-dimensional marginalised distributions we show the Overall (solid black), IMRPhenom (blue) and EOBNR (red) PDFs; the dashed vertical lines mark the 90% credible interval for the Overall PDF. The 2-dimensional plot shows the contours of the 50% and 90% credible regions plotted over a colour-coded posterior density function.

Source parameters for GW150914

	EOBNR	IMRPhenom	Overall
Detector-frame total mass $M/\mathrm{M}_\odot$	$70.3^{+5.3}_{-4.8}$	$70.7^{+3.8}_{-4.0}$	$70.5^{+4.6\pm0.9}_{-4.5\pm1.0}$
Detector-frame chirp mass $\mathcal{M}/\mathrm{M}_\odot$	$30.2^{+2.5}_{-1.9}$	$30.5^{+1.7}_{-1.8}$	$30.3^{+2.1\pm0.4}_{-1.9\pm0.4}$
Detector-frame primary mass $m_1/\mathrm{M}_\odot$	$39.4^{+5.5}_{-4.9}$	$38.3^{+5.5}_{-3.5}$	$38.8^{+5.6\pm0.9}_{-4.1\pm0.3}$
Detector-frame secondary mass $m_2/\mathrm{M}_\odot$	$30.9^{+4.8}_{-4.4}$	$32.2^{+3.6}_{-5.0}$	$31.6^{+4.2\pm0.1}_{-4.9\pm0.6}$
Detector-frame final mass $M_\mathrm{f}/\mathrm{M}_\odot$	$67.1^{+4.6}_{-4.4}$	$67.4^{+3.4}_{-3.6}$	$67.3^{+4.1\pm0.8}_{-4.0\pm0.9}$
Source-frame total mass $M^\mathrm{source}/\mathrm{M}_\odot$	$65.0^{+5.0}_{-4.4}$	$64.6^{+4.1}_{-3.5}$	$64.8^{+4.6\pm1.0}_{-3.9\pm0.5}$
Source-frame chirp mass $\mathcal{M}^\mathrm{source}/\mathrm{M}_\odot$	$27.9^{+2.3}_{-1.8}$	$27.9^{+1.8}_{-1.6}$	$27.9^{+2.1\pm0.4}_{-1.7\pm0.2}$
Source-frame primary mass $m_1^\mathrm{source}/\mathrm{M}_\odot$	$36.3^{+5.3}_{-4.5}$	$35.1^{+5.2}_{-3.3}$	$35.7^{+5.4\pm1.1}_{-3.8\pm0.0}$
Source-frame secondary mass $m_2^\mathrm{source}/\mathrm{M}_\odot$	$28.6^{+4.4}_{-4.2}$	$29.5^{+3.3}_{-4.5}$	$29.1^{+3.8\pm0.2}_{-4.4\pm0.5}$
Source-fame final mass $M_\mathrm{f}^\mathrm{source}/\mathrm{M}_\odot$	$62.0^{+4.4}_{-4.0}$	$61.6^{+3.7}_{-3.1}$	$61.8^{+4.2\pm0.9}_{-3.5\pm0.4}$
Mass ratio q	$0.79^{+0.18}_{-0.19}$	$0.84^{+0.14}_{-0.21}$	$0.82^{+0.16\pm0.01}_{-0.21\pm0.03}$
Effective inspiral spin parameter χ_eff	$-0.09^{+0.19}_{-0.17}$	$-0.03^{+0.14}_{-0.15}$	$-0.06^{+0.17\pm0.01}_{-0.18\pm0.07}$
Dimensionless primary spin magnitude a_1	$0.32^{+0.45}_{-0.28}$	$0.31^{+0.51}_{-0.27}$	$0.31^{+0.48\pm0.04}_{-0.28\pm0.01}$
Dimensionless secondary spin magnitude a_2	$0.57^{+0.40}_{-0.51}$	$0.39^{+0.50}_{-0.34}$	$0.46^{+0.48\pm0.07}_{-0.42\pm0.01}$
Final spin a_f	$0.67^{+0.06}_{-0.08}$	$0.67^{+0.05}_{-0.05}$	$0.67^{+0.05\pm0.00}_{-0.07\pm0.03}$
Luminosity distance $D_\mathrm{L}/\mathrm{Mpc}$	390^{+170}_{-180}	440^{+140}_{-180}	$410^{+160\pm20}_{-180\pm40}$
Source redshift z	$0.083^{+0.033}_{-0.036}$	$0.093^{+0.028}_{-0.036}$	$0.088^{+0.031\pm0.004}_{-0.038\pm0.009}$
Upper bound on primary spin magnitude a_1	0.65	0.71	0.69 ± 0.05
Upper bound on secondary spin magnitude a_2	0.93	0.81	0.88 ± 0.10
Lower bound on mass ratio q	0.64	0.67	0.65 ± 0.03
Log Bayes factor $\ln \mathcal{B}_{\mathrm{s/n}}$	288.7 ± 0.2	290.1 ± 0.2	—

重力波GW150914の7つの意義

① 一般相対論の強い重力場の初検証

② ブラックホールの地平線の初確認

③ 重い星質量ブラックホール（～30$M_{¤}$）の初確認

④ 連星ブラックホールの初確認

⑤ ブラックホール合体の初確認

⑥ ブラックホール合体が重力波で起こることを初確認

⑦ 超弦理論の古典リミットを決定

30M☉ブラックホールの合体
(Tagawa, Umemura, et al. 2016)

$$\dot{m}_i = \epsilon \dot{m}_{\mathrm{HL},i} = \epsilon \frac{4\pi G^2 m_{\mathrm{H}} n_{\mathrm{gas}} m_i^2}{(C_{\mathrm{s}}^2 + v_i^2)^{3/2}}$$

重力波(GW150914)検出

Advanced LIGO (Abbott et al. 2016)

$m_1 = 36^{+5}_{-4} M_\odot$　$m_2 = 29^{+4}_{-4} M_\odot$

- GW150914のブラックホール質量に合うのは，全て3体相互作用による合体
- 降着質量は，数M☉の寄与がある
- Pop Ⅲ 残骸の可能性

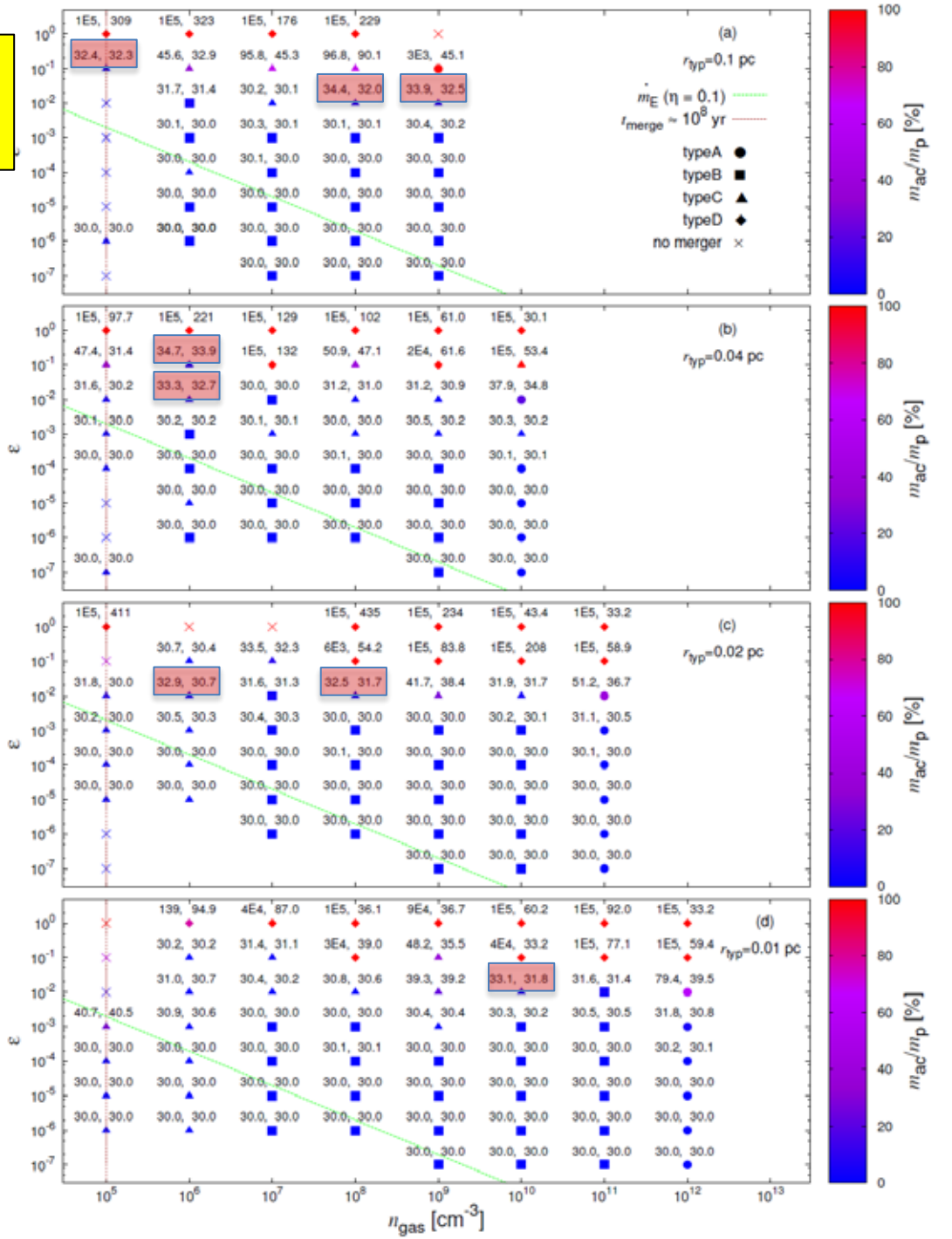

Astrophysical Implications

The formation of such massive black holes from stellar evolution requires weak massive-star winds, which are possible in stellar environments with metallicity lower than 1/2 the solar value.

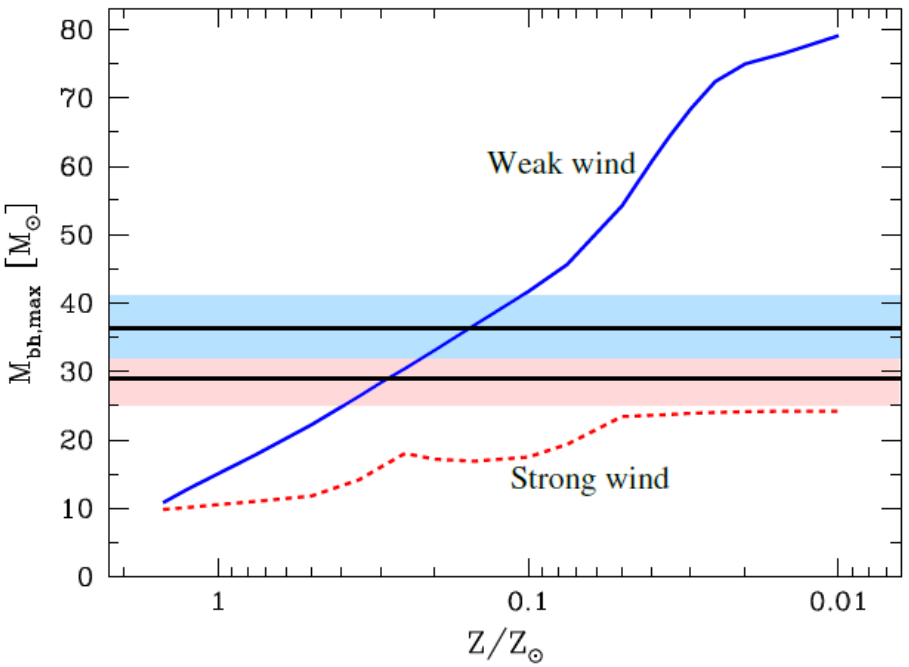

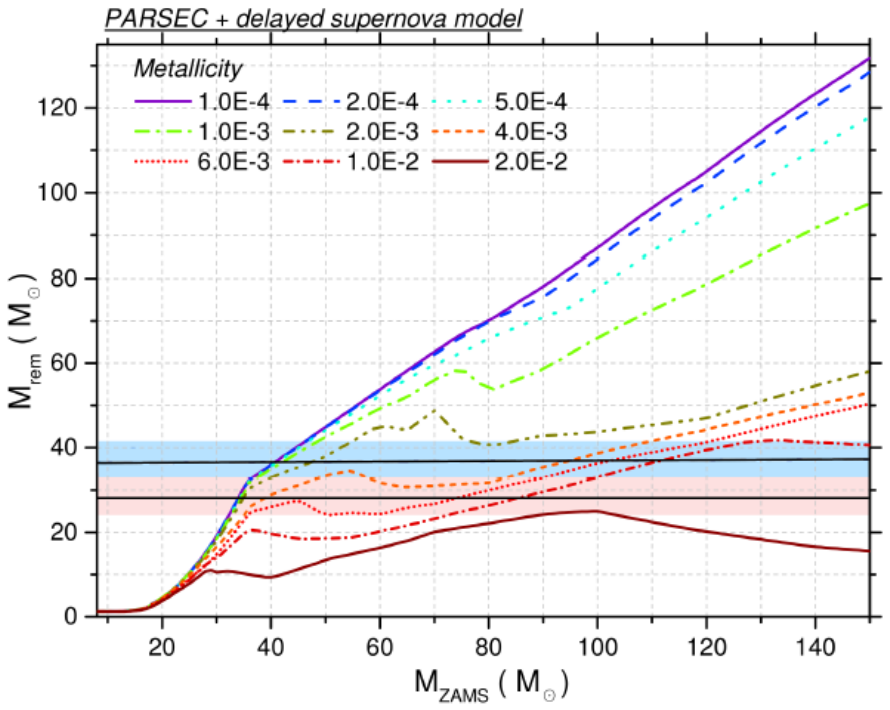

Figure 1. Left: dependence of maximum BH mass on metallicity Z, with $Z_\odot = 0.02$ for the old (strong) and new (weak) massive star winds (Figure 3 from Belczynski et al. 2010a). Right: compact-remnant mass as a function of zero-age main-sequence (ZAMS; i.e., initial) progenitor mass for a set of different (absolute) metallicity values (Figure 6 from Spera et al. 2015). The masses of GW150914 are indicated by the horizontal bands.

Counterpart in Hard X-Ray

Fermi GBM Observations of LIGO Gravitational Wave event GW150914

(Connaughton et al. 2016)

Ø GW150914 **の**0.4s**後に** >50 keV **で** weak transient source (a false alarm probability of 0.0022)
Ø Luminosity between 1 keV and 10 MeV = 1.8×10^{49} erg s^{-1}
Ø **方向ははっきり決まらないが,** GW150914**とは矛盾しない**
Ø **他の** astrophysical, solar, terrestrial, or magnetospheric activity **とは相関せず。**
Ø **weak short Gamma-Ray Burst を示唆**
Ø **これまで,** stellar mass black hole binary merger **から予想されていたわけではない。**

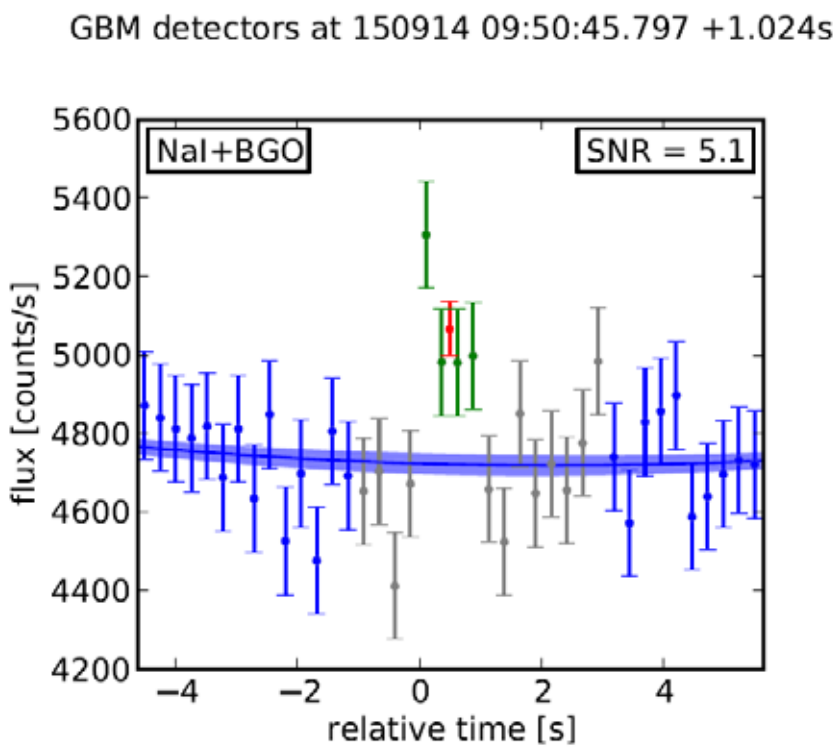

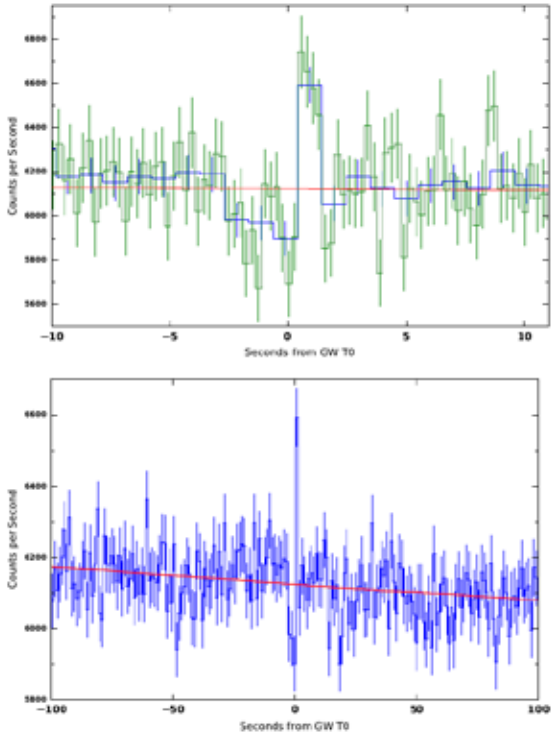

Mergers of Accreting Stellar Mass Black Holes

(Tagawa, Umemura, 2016 to be submitted)

Physical situation

初代星形成の3次元輻射流体計算

(Greif 2011, Susa 2013, Susa et al. 2014)

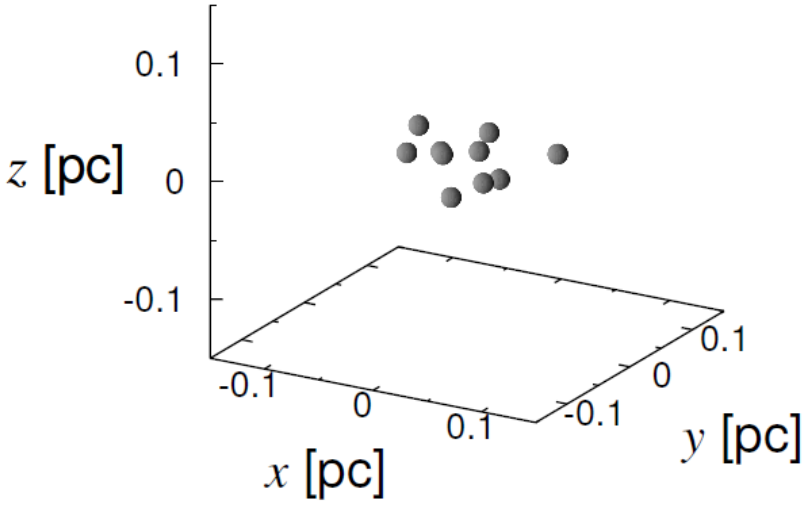

初期条件

- **ガス温度** T=1000 K
- **初期ガス質量** $M_{\rm gas}=10^5\,M_\odot$
- **BH質量** $m_{\rm BH}$=20, 25, 30 $M_\odot$
- **BH数** N=5
- **BH分布**：x-y**平面内に、ランダム**
- **BH速度**：$|\mathbf{v}_{\rm rot}|$　$|\mathbf{v}_{\rm random}|$
- **計算時間**：10^{10} yr
- **合体条件**：100 $r_{\rm sch}$

キーパラメーター

1. **初期ガス密度**$(n_{\rm gas})$
2. **初期BH密度**$(\rho_{\rm BH})$
3. **ガス降着率** $(\mathrm{e}=\dot{m}/\dot{m}_{\rm HL})$

BH初期質量依存性

Tagawa & Umemura, to be submitted

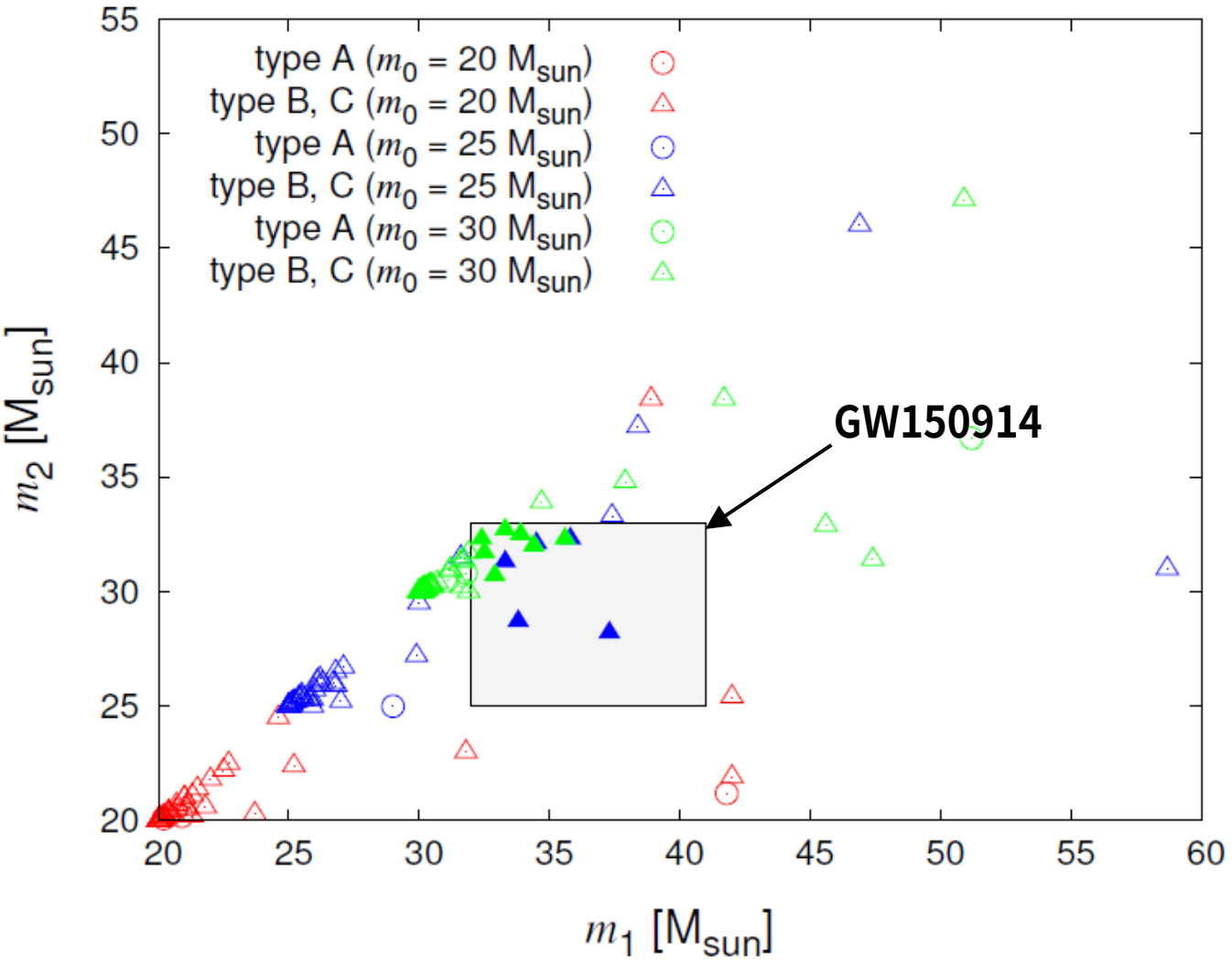

合体までの降着質量

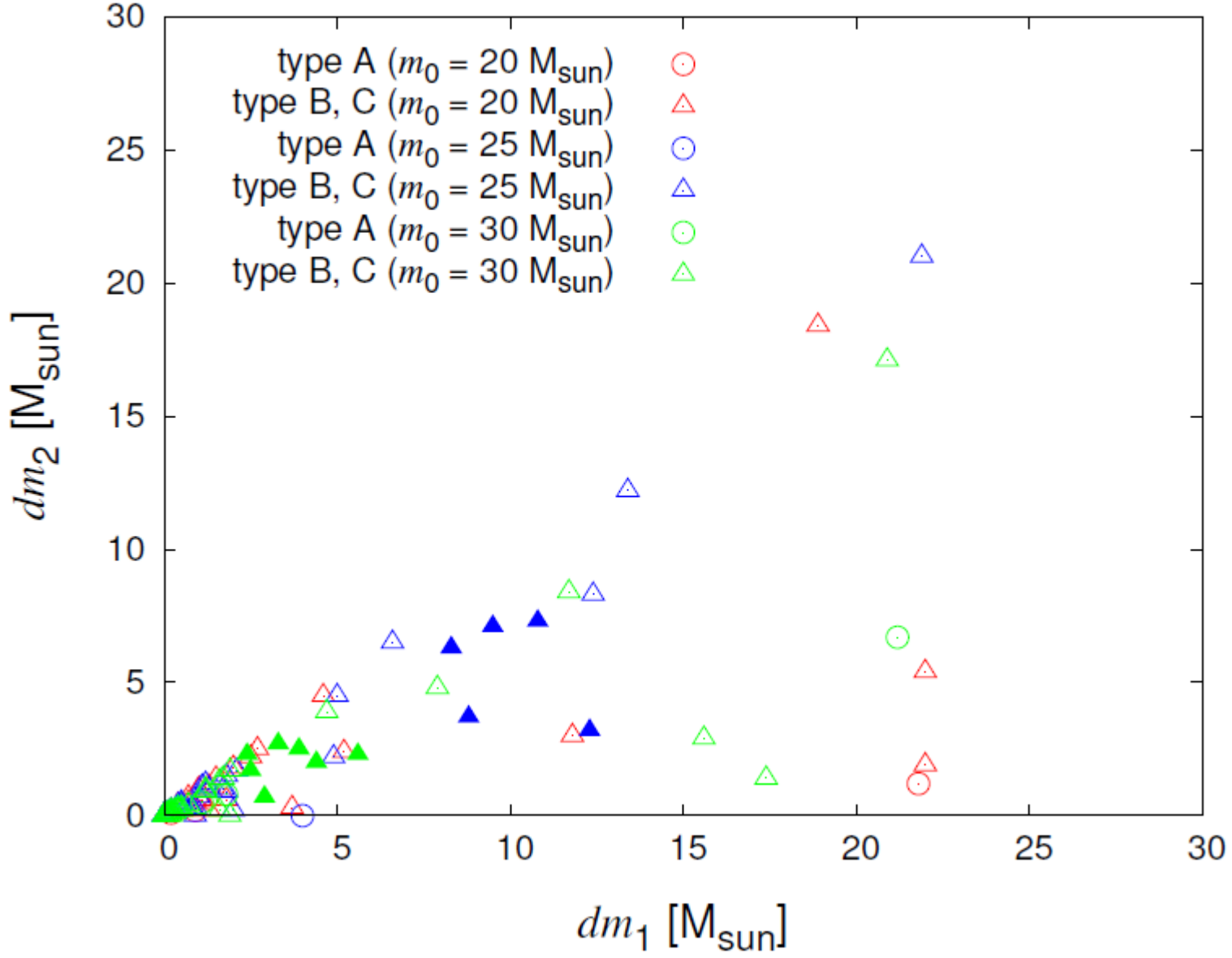
type A (m_0 = 20 M_{sun})
type B, C (m_0 = 20 M_{sun})
type A (m_0 = 25 M_{sun})
type B, C (m_0 = 25 M_{sun})
type A (m_0 = 30 M_{sun})
type B, C (m_0 = 30 M_{sun})
dm_2 [M_{sun}]
dm_1 [M_{sun}]
0
5
10
15
20
25
30

Conclusions

- **高密度ガス中の質量降着を伴うブラックホール合体で，GW150914を説明できる**

- **合体は，3体相互作用が支配的である**

- **初期質量は25M⊙以上，合体時までの降着質量は5－10M⊙**
  (Pop III remnants の可能性)